TÉCNICO LISBOA

Estimating Body Shapes From Body Measurements

Margarida Félix Lima

Thesis to obtain the Master of Science Degree in

Computer Science and Engineering

Supervisors: Prof. Joaquim Armando Pires Jorge
Prof. João António Madeiras Pereira

Examination Committee

Chairperson: Prof. António Manuel Ferreira Rito da Silva
Supervisor: Prof. Joaquim Armando Pires Jorge
Member of the Committee: Dr. Rafael Kuffner dos Anjos

November 2021

Acknowledgments

This thesis would not be possible without my Professors, Joaquim Jorge and João Pereira that guided me through the entire process. My sincere thanks go to Michael Hogg, the developer of *pygeodesic* library, for the tremendous help with the understanding oh his library and to Professors Stefanie Wuhrer and Brett Allen for their help in understanding some fundamental key points on their articles.

I would like to thank my parents for their friendship, encouragement and caring over all these years, for always being there for me through thick and thin and without whom this thesis would not be possible. I would also like to thank my grandparents, aunts, uncles and cousins for their understanding and support throughout all these years.

To each and every one of you – Thank you.

Abstract

E-commerce increases every single day, however it is still hard for people to buy clothes online because they have no idea of how they will look. To this end, we present an approach to model an approximation of a human body shape with a given set of body measurements in order to fit virtual clothes. To estimate a new body shape from body measurements we compared two different models that we developed. The first one uses linear transformations and the other uses *PCA* weights to estimate a new shape. Additionally, we selected the minimum number of body measurements required to perform an estimation with a similar shape as the ground truth. We evaluated our approach by comparing our results with estimations, and through visual evaluation via pictures and measurements taken from real people.

Keywords

PCA; Linear Transformations; Body Measurements; Shape Deformation.

Resumo

O e-commerce aumenta a cada dia, porém ainda é difícil para as pessoas comprarem roupas online porque elas não têm ideia de como elas ficarão. Para tanto, apresentamos uma abordagem para modelar uma aproximação da forma do corpo humano com um determinado conjunto de medidas corporais para caber em roupas virtuais. Para estimar uma nova forma corporal a partir de medidas corporais, comparamos dois modelos diferentes que desenvolvemos. O primeiro usa transformações lineares e o outro usa pesos *PCA* para estimar uma nova forma corporal. Além disso, selecionamos o número mínimo de medidas corporais necessárias para realizar uma estimativa com uma forma corporal semelhante à original. Avaliamos nossa abordagem comparando nossos resultados com estimativas e por meio de avaliação visual por meio de fotos e medições tiradas de pessoas reais.

Palavras Chave

PCA; Tansformações Lineares; Medidas Corporais; Deformação do Corpo.

Contents

List of Figures

List of Tables

1

Introduction

According to Digital Commerce 360 website, online apparel sales accounted for 38.6% of total U.S. apparel sales in 2019 and 100% of the growth in retail clothing sales. E-commerce's share of apparel sales has grown nearly 10 percentage points in the past 3 years, as online apparel sales accounted for 34.0% of total U.S. apparel sales in 2018 and 29.9% in 2017, according to Digital Commerce 360 estimates. The percentage of online shopping is increasing year after year, and e-commerce captured an even greater share of apparel sales throughout 2020 due to the coronavirus pandemic. As lockdowns became the new normal, businesses and consumers increasingly went digital, providing and purchasing more goods and services online, raising e-commerce's share of global retail trade from 14% in 2019 to about 17% in 2020 [5]. General e-commerce grew by leaps and bounds during the pandemic—a jaw-dropping 33.6% in 2020, to a total of nearly $800 billion. While e-commerce growth won't be as sky high in 2021, online shopping will still expand and accelerate far more than it did before shutdowns and social distancing. In fact, *Emarketer* [6] recently estimated that e-commerce will grow another 13.7% in 2021, reaching $908 billion [7]. In early 2021, the *EY Future Consumer Index* [8], which has surveyed thousands of consumers since the early days of the pandemic, found that 80% of U.S. consumers are still changing the way they shop. Sixty percent are currently visiting brick-and-mortar stores less than before the pandemic, and 43% shop more often online for products they would have previously bought in stores [9]. A survey by Engine [10]

found that people are spending on average 10-30% more online [11]. A research found that the top 500 retailer companies generated $849.5 billion in online sales in 2020, a 45.3% increase year-over-year and the biggest jump since *Digital Commerce 360* [12] began tracking the statistic in 2006 [13]. This means that the e-commerce is growing year after year, and the *COVID-19* [14] pandemic had a major impact on that growth.

However, many still prefer to buy clothes in a physical store instead of resorting to e-commerce [15–18], and one of the reasons is due to the fact that it is impossible to know how a piece of clothing would look when dressed [19–22]. This is because it is hard to model garments in a realistic way. To consider the fabric's physics, material, and texture, it is required a computational power that most devices do not possess yet. In addition, the amount of data needed in order to produce a realistic result is abysmal, which is monetarily expensive. Especially, data that requires high tech hardware like 3D scans, and several people to scan. The issue aggravates when privacy and ethical concerns are pointed out, specially because this data consists on the realistic shape of people's body including 3D models and/or photographs [23, 24]. Everyday new *deepfake* videos are uploaded to the internet and they are almost impossible to distinguish from reality. The ability of this technology to replace a person with another one likeness in a realistic ways have garnered widespread attention for their uses in celebrity pornographic videos, revenge porn, fake news, hoaxes, and financial fraud [25–28]. This proposal consists on modeling a human shape based on body measurements manually inserted by the user, and to model an undressed human shape, it is necessary to get naked examples and therefore it is necessary to scan people wearing the bare minimal amount of clothes - underwear. The acquisition of people that are willing to be scanned under those conditions can be hard, because it can be seen as an invasion of personal space. These are a few reasons on why there aren't more solutions to approach the realistic human body representation problem.

1.1 Contributions

We approached this problem by comparing two different models, one only using linear transformations and other using feature extraction, to see which is the best approach to model a new body shape from only body measurements. We also wanted to see if the usage of PCA was useful to map body shape with body measurements. We used polygon meshes that consist on a collection of vertices, edges, and faces that defines the shape of a three-dimensional object with flat polygonal faces, straight edges, and sharp corners or vertices - polyhedral object. These objects can be explicit once all vertex positions are defined in all axes, or implicit. An implicit surface is the set of zeros of a function of three variables. Implicit means that the equation is not solved for x, y or z. The usage of implicit surfaces would be valid in this thesis, however, this kind of surfaces are harder to handle and render, and since our dataset consists of explicit surfaces, it makes sense to use algorithms that apply to them.

Therefore, we modeled realistic 3D triangular meshes - meshes composed of triangular faces - of human bodies considering a set of body measurements, in an attempt to accurately output a polygon mesh with the exact same measures as the ones inserted by the user. Is important to highlight the fact that this thesis will focus on approaching the 3D modeling of a realistic 3D human mesh problem with focus on virtual garment fitting. Thus, it is vital that the estimated shape is as similar as possible to the original one.

There were two different aspects to evaluate the mesh quality in this proposal: the quality of the produced body shape and the body measurements of the final mesh. The first consists in directly comparing the final mesh with the estimated one by measuring the distance between the correspondent vertices of both meshes. Since we did not scan people to validate our approach, in the tests with real users we compared the final mesh with the users silhouette extracted from pictures. Thus, at the testing phase, the users needed to manually insert their body measurements as well as a photograph of themselves wearing minimal clothes. Finally, we also analyzed the body measurements of the final mesh and see how close they are to the original ones.

1.2 Project Goals

The goal of this thesis is to produce a realistic 3D model of a human body that considers a set of standard body measurements, e.g., height, waist, breast, and hips. These measurements are provided by the users, and the system will use them to produce a realistic 3D mesh that represents a human body with the specified measurements. We also defined what are the minimum body measurements required to produce a mesh with a similar body shape as the original one. We defined three goals for this thesis:

G1 To produce a realistic 3D model of a human body that considers a set of standard body measurements, e.g., height, waist, breast, and hips. These measurements are provided by the users, and the system will use them to produce a realistic 3D mesh that represents a human body with the specified measurements.

G2 To produce a realistic 3D model of a human body with the same body shape as the user using only their body measurements.

G3 To define what are the minimum body measurements required to produce a mesh with a similar body shape as the original one.

1.3 Results

To evaluate our approach, we calculated the the error of our representation facing the estimated results and see what are the relative errors. We also studied the reliability of the result facing the provided body measures, to see

if the new estimated shapes respected those measures or not. An analysis was made to see what are the minimal measurements required to accurately represent the result facing the estimation. We also visually evaluated the reliability of the mesh inspecting pictures.

At the end of this thesis, we developed an approach that is able to produce a mesh that respects a set of body measurements manually inserted by the users. The resultant meshes contained similar body measurements as the ones inserted and a body shape similar to the user that inserted the measurements.

We analyzed how many body measurements are in fact needed in order to represent the maximum amount of information. We concluded that seven measurements are enough.

1.4 Document Organization

This document first starts with a background where all concepts used to describe the thesis are specified at Chapter 2. Next is presented the related work at Chapter 3, in here we present the research performed for this proposal and highlight strategies that can benefit out approach. After that, we present our detailed proposed approach in Chapter 4 where all stages are specified and discussed. Finally, the evaluation methodology is detailed at Chapter 5 together with the limitations of our thesis.

2

Background and Theoretical Introduction

2.1 Body Measurements

Body measurements take a big role in this thesis, by being the main artifact to obtain new body shapes. We will reproduce real body shapes of real people by only providing their body measurements. They are fundamental in the fashion industry. To ensure that a finished garment will fit properly, it is important to take the following body measurements, so that you can determine what size you should make. It is always better to have someone else do the measuring. If that is not an option, you can measure a garment that fits you the way you want, and use these measurements as a guide. Most crochet and knitting pattern instructions will provide general sizing information, such as the chest or bust measurements of a completed garment. This thesis was developed with as a virtual fitting room in mind, therefore the body measurements can be used to model a new body shape but also to define which garment size that model benefits the most.

The size designation of clothes is an important aspect of the fashion industry, the standardization of sizes is a must. The International Organization for Standardization [29], or simply *ISO*, is a worldwide federation of national standards bodies (*ISO* member bodies). This organization is responsible for designing standard

methodologies or designations that normalize services or products, including clothing size labeling. The documents *ISO 5971:2017* [30], *ISO 8559-1:2017* [31], *ISO 8559-2:2017* [32] and *ISO 8559-3:2018* [33] detail extensively the norms that companies must follow to label a certain garment according to the human body measurements intervals.

Certain body measurements seem to be more used than others, regarding the fashion retailers. Waist, bust and hips girths are body measurements that are widely used. In this thesis we explore why some measurements are "better" than others regarding human body shape description.

2.1.1 Geodesic Distance

In geometry, a geodesic is commonly a curve representing in some sense the shortest path between two points in a surface [34], that can be represented by a graph. In the mathematical field of graph theory, the distance between two vertices in a graph is the number of edges in a shortest path connecting them. This is also known as the geodesic distance or shortest-path distance. Notice that there may be more than one shortest path between two vertices. If there is no path connecting the two vertices, e.g., if they belong to different connected components, then conventionally the distance is defined as infinite.

In this thesis, we assume that the geodesic distance between two vertices v_1 and v_2 is the sum of the lengths of all edges in the shortest-path between v_1 and v_2. The length of the edges is calculated using the Euclidean Distance [35]. The usage of geodesic distances will be fundamental in the extraction of the body measurements of the samples in the used dataset. The geodesic distance is detailed explained in Section 4.1.4.

2.2 Machine Learning

In this section, the machine learning techniques that were used in the thesis will be introduced. This is required in order the user to get familiarized with the used terms and the reason why we decided to implement those strategies.

First of all, Machine Learning is an application of Artificial Intelligence (*AI*) that provides systems the ability to automatically learn and improve from experience without being explicitly programmed. Machine learning focuses on the development of computer programs that can access data and use it to learn for themselves. There are plenty plenty categories of machine learning, such as: (a) Supervised Learning that can apply what has been learned in the past to new data using labeled examples to predict future events; (b) Unsupervised Learning are

used when the information used to train is neither classified nor labeled; (c) Reinforcement Learning is a learning method that interacts with its environment by producing actions and discovers errors or rewards. Trial and error search and delayed reward are the most relevant characteristics of reinforcement learning. However, we only consider supervised learning in this thesis, because we intend to learn something using information gathered before.

2.2.1 K-Nearest Neighbors (KNN)

A supervised machine learning algorithm (as opposed to an unsupervised machine learning algorithm) is one that relies on labeled input data to learn a function that produces an appropriate output when given new unlabeled data. The K-Neirest Neighbours algorithm, or simply *KNN*, is a supervised classification algorithm and assumes that similar things exist in close proximity. In other words, similar things are near to each other. The *KNN* algorithm hinges on this assumption being true enough for the algorithm to be useful. *KNN* captures the idea of similarity (sometimes called distance, proximity, or closeness) by calculating the distance between 2 samples in the sample space.

In *KNN*, *K* is the number of nearest neighbors. The number of neighbors is the core deciding factor, *K* is generally an odd number if the number of classes is 2. When *K=1*, then the algorithm is known as the nearest neighbor algorithm. This is the simplest case. Suppose P_1 is the point, for which label needs to predict. First, you find the one closest point to P_1 and then the label of the nearest point assigned to P_1. Suppose P_1 is the point for which label needs to be predicted. First, we find the k closest point to P_1 and then classify points by majority vote of its k neighbors. Each object votes for their class and the class with the most votes is taken as the prediction. For finding closest similar points, you find the distance between points using distance measures such as Euclidean distance, Hamming distance, Manhattan distance and Minkowski distance. In this thesis we use the Euclidean distance.

In summary, the *KNN* algorithm consists on: (1) Calculate the distances from P_1 to all other vertices of the dataset; (2) Find the k nearest neighbors; (3) Count the class of the k nearest neighbors, the final classification will be the most voted label. This algorithm will be used to assign vertices to the different human body parts.

2.2.2 Segmentation

To produce the best results with a supervised model, it is fundamental to have good data. This data needs to be well labeled, or in other words, with a correct classification tag. One of the strategies to reach this is segmentation. Segmentation is a technique with several industry applications: biology, geometry, linguistics, computer science and many other fields. In computer science field, it has plenty branches, since memory segmentation to

divide computer memory into segments, network segmentation to split a network into sub-networks, packet segmentation to divide a data stream into smaller units, or even in image segmentation to partition a digital image into multiple segments.

Lets take image segmentation as an example. In digital image processing and computer vision, image segmentation is the process of partitioning a digital image into multiple segments (sets of pixels, also known as image objects). The goal of segmentation is to simplify and/or change the representation of an image into something that is more meaningful and easier to analyze [36]. Image segmentation is typically used to locate objects and boundaries in images. More precisely, image segmentation is the process of assigning a label to every pixel in an image such that pixels with the same label share certain characteristics, like shown in Figure 2.1.

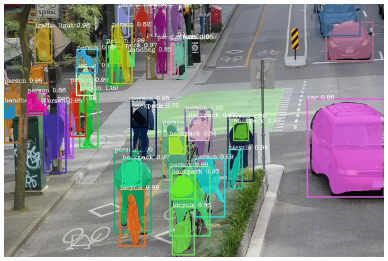

Figure 2.1: Segmentation and labeling of an image. In the image is represented a street filled up with people and cars. Some of the components in the image are segmented and labeled, For instance all people with a visible body are labeled as "person". Some of them are wearing a backpack, which is also considered by the labeling system, as well as the bicycles, cars and traffic lights.

The result of image segmentation is a set of segments that collectively cover the entire image, or a set of contours extracted from the image. Each of the pixels in a region are similar with respect to some characteristic or computed property, such as color, intensity, or texture. Adjacent regions are significantly different with respect to the same characteristics. In Figure 2.2 is represented the result of segmenting an image. A detailed explanation is given on how segmentation is used in this approach at Section 4.1.3.

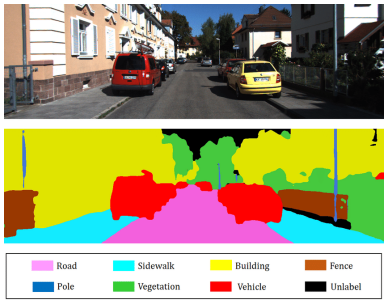

Figure 2.2: Segmentation of an image into different segments. On the top is the original image of an ordinary street with cars and houses. At the bottom is represented all segments of the original image with representative colors: everything that is represented as green is vegetation, red elements are vehicles, yellow are buildings, etc.

2.2.3 Curse of Dimensionality

At the first glance, a dataset with several features might be a good thing. A supervised model benefits from data, and the more data, the better, right? Well, not really. As the dimensionality of the feature space increases, the number of configurations can grow exponentially. This is called *Curse of Dimensionality* and it can lead to several anomalies that would not happen in a low dimension environment [37].

Those anomalies can be prevented by removing some feature variables to decrease the number of variables used in a model, and therefore its complexity. To do this, we extract the information of the dataset and create a new one that has the same information as the original one - feature extraction - or we can simply select a subset of features of the original dataset - feature selection. Both methods work, and both have advantages and disadvantages. The key difference between feature selection and extraction is that feature selection keeps a subset of the original features, while feature extraction creates brand-new ones that have no connection to the original features at all.

In this thesis, we do not deal with the *Curse of Dimensionality* phenomena, because we only have 41 distinct features. These features represent a set of body measurements that were extracted from synthetic meshes, however to ask someone to extract 41 body measurements from their body is too much. Thus, reducing the features leads, most of the time, to better results when it is done correctly.

Feature Selection

Feature selection is useful for filtering irrelevant or redundant features from a dataset. The key difference between feature selection and extraction is that feature selection keeps a subset of the original features while feature extraction creates brand-new ones.

There are plenty of feature selection methodologies that fall under the supervised or in the unsupervised spectrum. The supervised methodologies all require a feature that is considered as the target, or in other words, that feature is considered the one that determines the class of samples. However, our dataset is composed of 41 features that are the body measurements of human beings, and there is not a labeling feature. We are not classifying the gender of the sample, or their age. We are establishing a map between body measurements and human body shape. Thus, supervised feature selection do not fit our needs. On other hand, unsupervised feature selection methodologies do not need a labeling feature to reduce the features of the dataset.

All unsupervised methods rely on analyzing the dataset that they are trying to reduce. We used variance and correlation. Variance consists on analyzing the distribution of the features of the dataset and remove the

features that vary less than a certain threshold. If a certain feature has a similar value at all samples, it does not help to differentiate it, therefore we can remove that same feature without any significant loss of information. Correlation is a bit more complicated, as it will relay on how correlated certain features are. If you have a dataset that has the measurement of the left leg and the measurement of the right leg, as well, in humans, both features will be highly correlated. This means that if the value of the left leg measurement increases, the value of the right leg measurement increases as well. In humans, both legs have relatively the same length, which means that by adding both measurements as features of a dataset, we would be adding redundancy. We would only have more processing time and complexity for no extra information at all. Thus, we excluded one of those features. That is, what correlation does, it discovers relations between variables. We can exclude features from our dataset that are highly correlated with other features. In the end, the final subset of features should not be correlated at all, to be able to describe the maximum of information as possible, for the less space and processing as possible.

Feature Extraction

The main linear technique for feature extraction is principal component analysis and performs a linear mapping of the data to a lower-dimensional space in such a way that the variance of the data in the low-dimensional representation is maximized. In practice, the covariance matrix of the data is constructed and the eigenvectors of this matrix are computed. The eigenvectors that correspond to the largest eigenvalues (the principal components) can now be used to reconstruct a large fraction of the variance of the original data. Moreover, the first few eigenvectors can often be interpreted in terms of the large-scale physical behavior of the system, because they often contribute the vast majority of the system's energy, especially in low-dimensional systems. Still, this must be proven on a case-by-case basis as not all systems exhibit this behavior. The original space (with dimension of the number of points) has been reduced (with data loss, but hopefully retaining the most important variance) to the space spanned by a few eigenvectors.

To produce a supervised learning model, a dataset may contain a large number of variables, what complicates the analysis of the information. Imagine a dataset with 1000 variables, every time that is required to perform any kind of calculation, a vector with 1000 dimensions is used. This would lead to vast computations every time a calculation was performed. Therefore, a strategy to decrease the number of variables is required.

Principal Component Analysis, or simply *PCA*, is a dimensionality reduction method that is often used to reduce the dimensionality of large datasets, by transforming a large set of variables into a smaller one that still contains most of the information in the large set. Reducing the number of variables of a data set naturally comes at the expense of accuracy, but the trick in dimensionality reduction is to trade a little accuracy for simplicity. Because smaller data sets are easier to explore and visualize and make analyzing data much easier and faster for

machine learning algorithms without extraneous variables to process.

Principal components are new variables that are constructed as linear combinations or mixtures of the initial variables. These combinations are done in such a way that the new variables (principal components) are uncorrelated and most of the information within the initial variables is squeezed or compressed into the first components. Therefore, the idea is 10-dimensional data provides you 10 principal components, but *PCA* tries to put the maximum information as possible in the first component, then the maximum remaining information in the second, and so on, until having something like shown in the Figure 2.3.

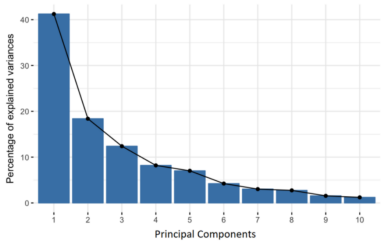

Figure 2.3: A plot showing the amount of variance explained by each principal component, the more variance a component explains, more information that component contains. The first principal component is the one with more information with a bit more than 40%, followed by the second that explains more 19% and so on. It is visible that the first 6 (six) principal components are enough to explain more than 95% of information in a dataset.

Geometrically speaking, principal components represent the directions of the data that explain a maximal amount of variance, that is to say, the lines that capture most information of the data. The relationship between variance and information here, is that, the larger the variance carried by a line, the larger the dispersion of the data points along it, and the larger the dispersion along a line, the more the information it has. To put all this simply, just think of principal components as new axes that provide the best angle to see and evaluate the data, so that the differences between the observations are better visible.

3

Related Work

Body representation has always been a major subject in computer graphics. Until very recently, it has been used almost entirely in the gaming industry, to create characters as realistic as possible. Amaury and Daniel Thalmann describe in [38] that there are two major models that are used to represent the human body: surface models and multilayered models. Both models are composed by a skeleton and a skin representation, which can be a triangular mesh or a set of surface patches. With that, it is possible to add deformation functions to simulate the joint movement to add realism to an avatar's animation.

Since that this thesis mainly focuses on parametric models of the human body, the research was also focused on that direction. In this specific case, the parameters are measurements of an individual's body such as height, length of the legs, arms, etc. Those inputs can be manually inserted by the user [39–42], or the parameters could be learned from a 3D scanned human mesh dataset [1, 39–41, 43–48], a RGB image [1, 43, 49] or even a binary image [47]. Once the system obtains those parameters, the next step is to model the mesh accordingly to those parameters.

The modeling of a human body is a hard task to accomplish. Recently there's a lot of work in supervised learning done that involved the 3D scanning of plenty bodies [1, 45, 47, 48] that were later used to estimate a body deformation in a variety of poses [44–46, 48, 50], or just simply to map an image to a 3D model from a single image [1, 3, 43, 47, 49].

3.1 Surface Models

A surface model is either a triangular mesh or a set of surface patches, whose deformation is driven only by the motion of an underlying hierarchical structure or skeleton. That means that in Figure 3.1 a surface model would only consist of the red and beige layers. This kind of model is still mainly used, especially in the gaming industry, because it is much more computationally cheaper, despite the fact that the results are not considered the best. This subsection is divided into three parts: estimating body measurements as parameters, mesh modeling and deformation and mesh animation. The first part talks about approaches that estimate body measurements by plenty of means, mainly 3D scanned meshes or images, and estimates a 3D mesh that best applies to those values. The second part of this section references used techniques that deform meshes, preferentially respect a set of parameters, or body measurements in this case. The third and final part will identify some approaches proposed to deform 3D meshes with different shapes depending on the body pose.

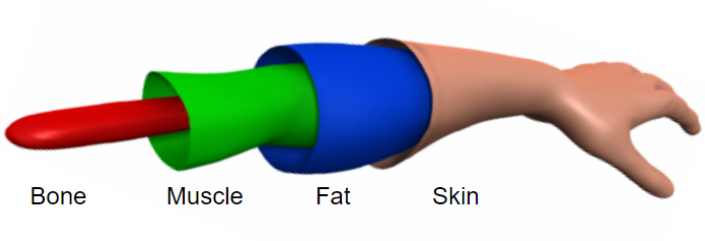

Figure 3.1: Visual representation of an arm composed by four different layers, from left to right: bone (red), muscle (green), fat (blue), skin (beige).

Currently available approaches can be divided into two main categories: feature matching where a system directly regress a 3D geometry from images, and template adaptation where the system deforms a template mesh to respect a set of input parameters.

3.1.1 Feature Matching

Non surprisingly, the majority of recent work done in creating parametric avatars has been accomplished using a mesh database derived from 3D scanned bodies of real people. However, this process is expensive because it

requires some high-end gear.

After scanning the necessary meshes, one of the options is to train a system that either estimates body parameters, where given some input, the system would output the body measurements as parameters to estimate the desired body shape. The usage of neural networks proved to be efficient in this topic. In *PIFuHD* [1] it is used a neural implicit functions for shape representation, see Figure 3.2 to see some results. in *HS-Nets* [47], the parameters themselves are computed based on images as input, and are used to reconstruct the 3D human shapes by using a statistical human shape model based on *SCAPE* [44], see Figure 3.3 to see some results. This model was proposed in 2005 and the shape variation is represented by using *principal component analysis (PCA)* on a set of 3D scans of different people in different poses, which includes a low-dimensional subspace of body shape deformations.

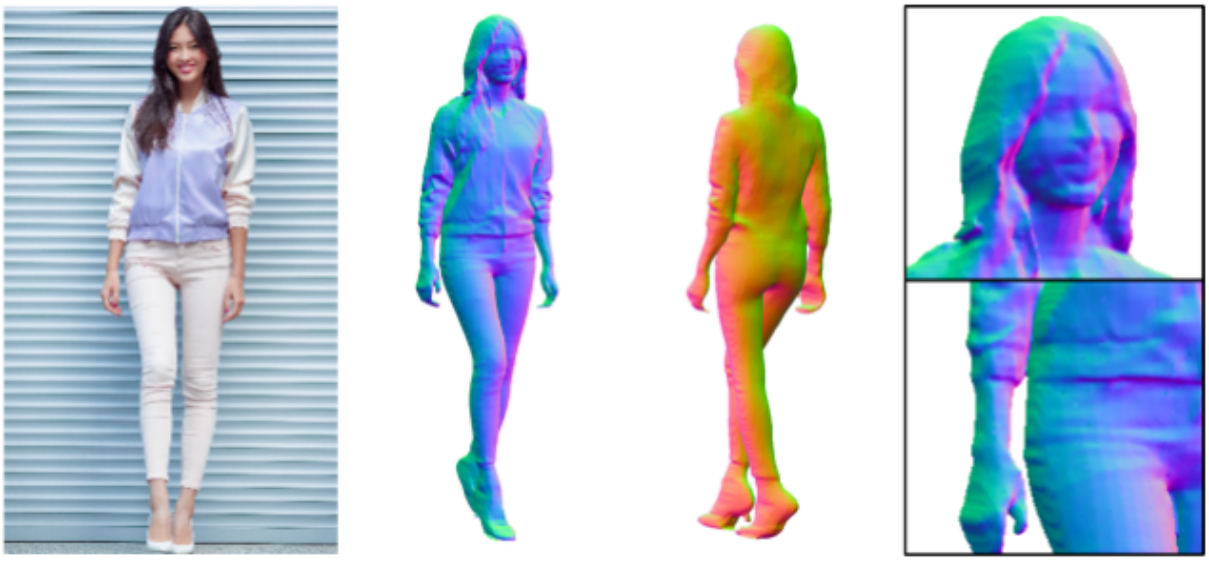

Figure 3.2: Results of *PIFuHD* [1] after inferring 3D geometry of clothed humans at 1k image resolution in a pixel-aligned manner, retaining the details in the original inputs without any post-processing.

In *HS-Nets* however, to learn the global mapping from the data to the parameters, a convolutional neural network (*CNN*) is trained. This CNN is trained by feeding the images from different views into the network, however the images are concatenated by a merge layer that performs a max operator over each dimension. However, by outputing a 3D mesh with this system might lead to a wrong human body shape representation by misleading its body measurements. This proposal designs a model that receives body measurements as input and outputs a realistic 3D mesh representation of a human 3D mesh with the measurements as constraints. The same argument is applied to *Detailed Human Depth Network (DHDNet)* [49], where Zhang uses *CNN*s in order to estimate a detailed and completed depth map from a single *RGB* image that contains occlusions of human body. Since information is retrieved from an RGB image, there is no certains that the outputed body representation of

Figure 3.3: Mesh reconstruction for 4 real subjects in mildly varying poses. (left) Input image (middle) Extracted Silhouette (right) Reconstruction of the estimated shape.

the individual in the image respects its body measurements. The estimation of a 3D mesh from an image could be useful to evaluate the thesis by calculate the differences between the mesh obtained from this proposal and the mesh estimated by the *CNN* model, however that process will not be used because as said previously, this systems do not consider the body measurements of the person in the picture as a parameter.

3.1.2 Template Adaptation

After obtaining the desired parameters, that in this case correspond to body measurements, either by estimating those values using machine learning, or by manually inserting them into the system, it is necessary to create a 3D model based on those values.

The usage of blend shapes allows an approach without requiring any machine learning technique. Morphing requires a final model shape (target) to be able to morph from the base shape until the desired one. The disadvantage of this kind of process is that it requires a lot of modeling by the developers to have one or more target meshes.

One example is *HMR* [43], Zhang builds a standard model to be deformed in three different levels and to recover occluded surface details using the depth information, see Figure 3.4 to see some results. Both *HMD* [3] and Seo in [40] use blend shapes to update the shape of a model in real time by using an iterative interface.

IntExMa [41] uses a morphing algorithm to comply with the desired body measurements as input. Morph targets are used to define vectors for the deformation of a defined set of vertices in the complete model. The deformations are made in an automatic iterative process that ends up with a model that fits the desired proportions. Another example is [45] where blend shapes are used not only for body poses but also for poses with more details about the body pose in Section 3.1.3.

Figure 3.4: Human Mesh Recovery (HMR): End-to-end adversarial learning of human pose and shape. The authors describe a real time framework for recovering the 3D joint angles and shape of the body from a single RGB image. The first two rows show results from our model trained with some 2D-to-3D supervision, the bottom row shows results from a model that is trained in a fully weakly-supervised manner without using any paired 2D-to-3D supervision. They also infer the full 3D body even in case of occlusions and truncations.

SMPL [45] is a skinned vertex based model that accurately represents a wide variety of body shapes in natural human poses. This model contains four main elements: a template mesh (T), shape blend shapes, pose blend shapes and a pose. A template mesh in a T-pose is used, the output will be this same mesh into a certain given pose, where the body shape depends oh that given pose, e.g. if the pose is being sit the belly would pop out a bit more. Shapes blend shapes consist of offsets applied to T in order to represent new body shapes and post dependent shape changes. From training 3D scans of real people in T-pose, shape blend shapes from different parts of the human body are learned to capture human shape variation using *principal component analysis (PCA)*. This results on the principal modifiers that act on mesh's shapes, or by other words, returns the components that most change in the provided dataset. Learning the human body shape through *PCA* is a strategy used by a lot of projects [39, 40, 44–46, 48] and it is an effective strategy to learn the variation between different human body shapes, that is why this strategy will be used in this proposal as well to learn the blend shapes that most realistic modify a human 3D mesh.

In [39] the data base is clustered and statistically analyzed to capture the tendency of body shape variation, and from that tendency the body shape parameters are extracted. One of the meshes is considered to be the basis of registration, or in other words, the ground truth. The mesh's input body sizes are classified into groups and the parameters (body measurements) of that group are taken into account at the R3 $\longmapsto$ R3 transformation that is applied to the base mesh in order to output a new mesh with the desired input measurements. The usage of a ground truth seems wise, because that way exists an initial mesh to work with. Seo in [40], uses a template mesh as well by using a database of 3D scanned meshes from real people, and it is used as examples to correspond a template mesh deformations with the body measurements. In fact, the usage of 2 templates (one male and the other female) could be beneficial to generalize each gender better. A third neutral gender could be used as the average of the entire dataset instead of the average of just one gender. Having this, it is possible to apply transformations (in this case, blend shapes) to that mesh to represent a different body shape.

3.1.3 Animating Body Meshes

The final part is to add movement to a certain mesh, but more importantly is to know how to represent that mesh in different poses. A realistic animation deforms a mesh depending on the body pose and body shape. A very popular approach to this problem is the usage of regression on joints to increase animation correction and realism.

Besides the rest pose template, blend weights, pose-dependent blend shapes, and identity-dependent blend shapes, *SMPL* [45] also contains a regressor from vertices to joint locations. Unlike previous models, the pose-dependent blend shapes are a linear function of the elements of the pose rotation matrices. This simple formulation enables training the entire model from a relatively large number of aligned 3D meshes of different people in different poses. It predicts the joint positions for a given body shape as a function of the mesh vertices. Pose blend shapes are learned from training 3D scans of real individuals in a variety of poses, this captures how real bodies differ from blend skinned bodies, and allows the system to learn how to model body meshes segments (different parts of the body) as pose dependent. Given a pose that is provided to *SMPL*, it computes the near contribution of this blend shape, the correct skinning errors and produce realistic pose dependent deformations. Finally the *SMPL* use of standard blend skinning to transform the deformed template shape into the desired pose.

STAR [46], being the evolution of *SMPL*, is 80% smaller because it uses far less parameters by defining per-joint pose correctives and learn the subset if meshes vertices that are influenced by each joint movement. This sparse formulation results in more realistic and general deformations and significantly reduces the number of model parameters to 20%. The system learns shape-dependent pose-corrective blend shapes that depend on both body pose and body mass index (BMI), which was huge compared to *SMPL*, since it factors pose-dependent

deformations from body shape while, in reality, people with different shapes deform differently. *STAR* also differs from *SMPL* by being trained with an additional 10000 scans of male and female subjects (being added a neutral gender optimization recently), which improves model generalization. Just like *SMPL*, STAR also uses a joint blendshape regressor that allows poses to look realistic. This regressor however, is more compact than the previous one by using a diferent representation, which contributes to the significative reduction of parameters on STAR comparatively to *SMPL*.

The consideration of the pose to deform a mesh is a valuable artifact, however it is not the primal concern of this thesis. This is a desirable feature that would allow a more realistic virtual dressing by performing animations that a person would do personally in the dressing room, e.g., sitting, jumping, etc. Therefore we do not consider pose variation in this thesis.

3.2 Multi-Layered Models

This kind of model takes into consideration that there are several types of body tissues that behave differently. Therefore, this model will differ from the previous one by adding more layers to it (just like the name suggest). A multilayered model is not just composed by a skeleton and a triangular mesh. It is also composed by some intermediary layers such as muscle and fat layer, just as seen in Figure 3.1. Here, the motion due an underlying hierarchical structure or skeleton is also applicable, but instead of being directly from the skeleton to the skin, it passes through two intern layers.

This way, when the skeleton moves, that motion will be reproduced by the muscle layer first, then the fat layer, and finally the skin reproduces the result of them all. In terms of animation, this kind of model produces a much better result than a simple surface model, especially when each layer is modelled accordingly.

Multi-layer Lattice [2] achieve that in a really effective way using voxels. A voxel can be seen as a correspondence of a pixel but in a three-dimensional space, therefore it represents a value on that grid and in this case, that value will identify that specific voxel as bone, muscle, fat or skin. This way, with a mesh as an input, this mechanism was useful to fill the interior and to get separated layers without any extra modeling work as seen in Figure 3.5.

This procedure was especially interesting for this thesis because the layer classification was made based on inputs that the user would insert, including bone width and muscle-to-fat ratio, just like it is pretended. It was also possible to define such parameters in a body part level, such that the different parts of the character can behave differently during the simulation. For instance, there are characters that contain more fat in the

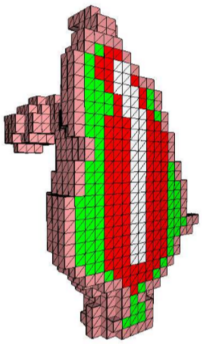

Figure 3.5: Implementation of the multi layered model using voxels as proposed on [2].

belly than in the legs. The differentiation between layers is useful for animation purposes, in which a layer behaves accordingly to a certain model. For instance, the fat layer should be much more elastic than the muscle one, since the fatty tissues hang loosely under the action of gravity. This model results in more computational complex but much more realistic animations.

Simulating both muscle and fat layers could add some realism to this thesis, since it is intended to simulate garments with an avatar. Having both layers reacting to external forces would add realism to the dressing experience, since the avatar would react to the clothes in a more realistic way. For instance, if you have an avatar and two pairs of jeans: one of a small size and another of a large size, the avatar would react differently to both of them. Since the fat layer would be dynamic, the smaller pair would be tighter than the larger one and that would reflect on the avatar by squishing it and deforming its body.

Another approach is to use premodeled parts and adjust them to the inside of the input mesh, what is precisely what Michael Pratscher did on *Outside-In* [51]. In similarity to *Multi-layer Lattice*, *Outside-In* also receives a mesh as an input and the insides are filled, in this specific case, with artificial muscles. The user can then change the muscle sizes in order to give the avatar the desired shape. Contrary to *Multi-layer Lattice*, this thesis only considers the muscle layer. This kind of approach would definitely add more realism to the virtual mannequin, because each user could customize their avatar in their own way, but since the virtual mannequin should be as realistic as possible, the fat layer should not be ignored.

Despite the fact that a multi-layered model would result in a more realistic outcome, adding a soft tissue layer is a desirable feature for future work and it is not considered on the thesis. Therefore, it won't be part of the proposal itself, instead it will be on the future work.

3.3 Summary

As a summary of the entire section of related work, Table 3.1 was created with all important references of the related work referring all important aspects of this thesis. In the table it is visible that all projects consisted of deforming a mesh (see column "Shape Deformation" of Table 3.1). All projects used a 3D scanned dataset of human meshes, except [3, 49] (see "3D scanned Dataset" column of Table 3.1). Referring to the human shape, there are some projects that analyze the human shape variation and there are others that do not, the ones that do [39, 40, 44–46, 48] use the results to model an humanoid mesh to make it look more realistic. However, only one project takes into consideration the body measurements that are manually inserted by the user. Volz, Blum, Hämberling and Khakzar, in *IntExMa* [41], present an approach based on transformation functions that models a template mesh into a desired set of body measurements. The usage of manually inserted body measurements makes *IntExMa* the most similar project to this thesis, however, it does not consider the human shape variation. This thesis considers human shape variation as an heuristic of mesh deformation, that leads to more realistic results.

		Usage of Body Measures			
	3D Scanned Dataset	*Manual*	*Estimated*	*Shape Variation*	*Shape Deformation*
This thesis	✓	✓	✗	✓	✓
Parametric Human Body Shape Modeling for Human-Centered Product Design [39]	✓	✗	✗	✓	✓
End-to-end Recovery of Human Shape and Pose [43]	✓	✗	✗	✗	✓
Automatic, Body Measurements Based Generation of Individual Avatars Using Highly Adjustable Linear Transformation [41]	✓	✓	✗	✗	✓
SCAPE Shape Completion and Animation of People [44]	✓	✗	✗	✓	✓
SMPL A Skinned Multi-Person Linear Model [45]	✓	✗	✗	✓	✓
STAR Sparse Trained Articulated Human Body Regressor [46]	✓	✗	✗	✓	✓
PIFuHD Multi Level Pixel Aligned Implicit Function for High Resolution 3D Human Digitalization [1]	✓	✗	✗	✗	✓
An Automatic Modeling of Human Bodies from Sizing Parameters [40]	✓	✗	✗	✓	✓
HS-Nets Estimating Human Body Shape From Silhouettes with Convolutional Neural Networks [47]	✓	✗	✗	✗	✓
Parametric 3D modeling of a symmetric human body [48]	✓	✗	✗	✓	✓
See through Occlusions Detailed Human Shape Estimation From a Single Image with Occlusions [49]	✗	✗	✗	✗	✓
Detailed Human Shape Estimation from a Single Image by Hierarchical Mesh Deformation [3]	✗	✗	✗	✗	✓

Table 3.1: Summary of the related work referring to Section 3.3

4

Our Approach

This thesis contemplate the study of human body shape variation and relate those variations to the body measurements. We differ from the projects cited in the Related Work Section 3.3 by performing feature analysis on the body measurements dataset to obtain a subset with measurements that better represent the human body shape variation. We distinguish ourselves from most projects represented in Table 3.3 for using body measurements to accurately estimate a human shape.

To approach the problem of estimating a new body shape based on body measurements, our technique is divided in three major sections as shown in Figure 4.1: preprocessing, model generation, and evaluation. The first step is to preprocess the dataset. In this step, the template models are created, measured, and analyzed in terms of their body measurements and coordinates. With that information, it is possible to create a mesh of any shape given a set of body measurements as input.

In the first stage, the *Semantic Parametric Reshaping of Human Body Models* [4] we preprocessed the dataset to be used in the next steps, and it begins by repairing the meshes. This is an essential step as it prevents any mistake that might happen while extracting the body measurements. After reparation, all meshes will be

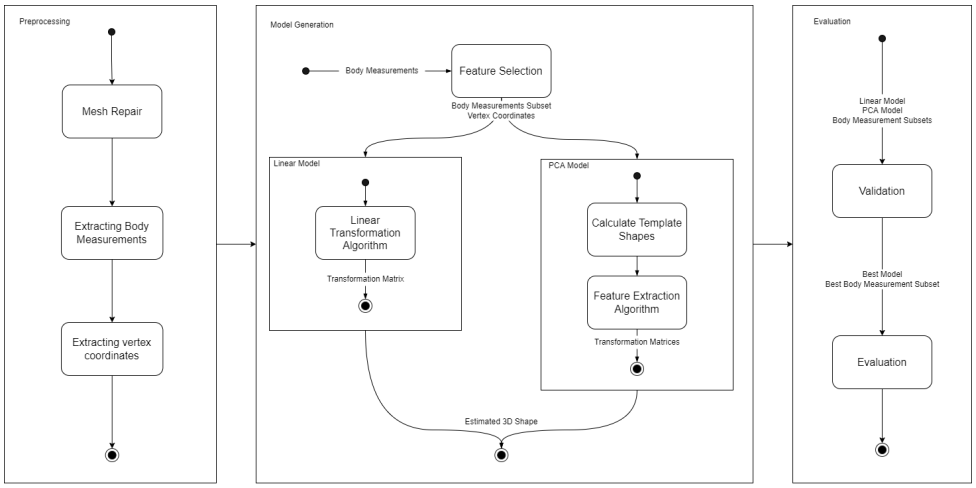

Figure 4.1: Overview of the proposed framework. The dataset is preprocessed where the template meshes are calculated and the primary features are extracted. As soon as the framework has this information, it is possible to deform the template model according to a set of body measurements. This procedure will then be compared with an estimated mesh resulting from [3] by calculating the mean square error between both meshes.

segmented into sub-meshes, where each sub-mesh represents a different part of the body (torso, upper leg, lower leg, etc). Since the dataset only contains meshes, without any landmarks, like height, arm length, leg length, waist, etc, it is necessary to extract those distances ourselves. That was accomplished by using three different distances between points on the mesh: length, height, and girth. The usage of distances like geodesics is important because it takes into consideration the mesh surface to compute the distance. It simulates what a tailor would do while measuring people. The measurements are be useful to learn how different body parts deform, and to apply deformations based on body measurements that users manually insert into the system. After this, the model generation module can initiate.

The learning process is marked by two different models that will be compared with each other. The first one uses feature extraction to learn the principal components that vary in a human body, relate it to the body measurements, and apply the learned model to new sets of body measurements. The other model only uses feature selection to learn which subset of body measurements describe human shape the best. It learns a model for that subset and applies it to any new subset that is inserted. Both models receive body measurements as input that they use to learn how human body shapes vary based on body measurements, and output an entirely new shape based on the inserted measurements.

4.1 Preprocessing

Preprocessing refers to the manipulation or dropping of data before it is used to ensure or enhance performance. It removes unwanted data that has no value to the performance of a certain process. This outputs a dataset that contains more valuable information after the preprocessing stage for data manipulation later in the process. Editing such dataset to either correct data corruption or human error is a crucial step to get accurate quantifiers.

The input of the preprocessing module are the meshes of the *Semantic Parametric Reshaping of Human Body Models* [4], and the output are two new datasets computed from the original one: the vertex coordinates of each mesh, and the body measurements of each mesh. In this Section, we explain how those tables are calculated to recreate a 3D mesh of a human body entirely based on body measurements. This first step is to clean the samples itself, correct any geometry imperfection that they might have: internal faces, non-manifold vertices, etc. How that is achieved is explained in Section 4.1.2. The preprocessing continues in the Section 4.1.3, where the segmentation process is explained. The final step of the preprocessing is to create the required datasets from the 3D meshes, that is explained in the Section 4.1.4.

4.1.1 Dataset

This thesis proposes to model human bodies using solely provided body measurements as input. However, to do that in a realistic way it is necessary to extract information from a trustworthy source. The ideal dataset for this thesis would be the one that contains 3D scanned meshes from several individuals in T-pose, together with 1D measurements (landmarks) that represent body measurements. *Civilian American and European Surface Anthropometry Resource (CAESAR)* dataset contains all this, but it is a commercial version that is not freely available for research purposes.

To extract information about human shape variation, Yipin Yang results in *Semantic Parametric Reshaping of Human Body Models* [4] were used. The dataset is composed of around 3000 meshes, where 1500 are male and 1500 are female. Each mesh contains 12500 vertices and all meshes are positioned in a neutral pose as shown in Figure 4.2. However, the pose of all meshes is slightly different due to human errors. For instance, if two different people were asked to position themselves in the position represented by the mesh of Figure 4.2 the final pose would always differ from person to person because of the angle of the arms or even the position of the feet. This means that the dataset is not perfect as it contains pose differences that can compromise the body measurements and the overall results. We do not consider the pose in this thesis.

In [4], the authors developed a novel approach to generate human body models in a variety of shapes and poses via tuning semantic parameters. The approach is investigated with datasets of up to 3000 scanned body

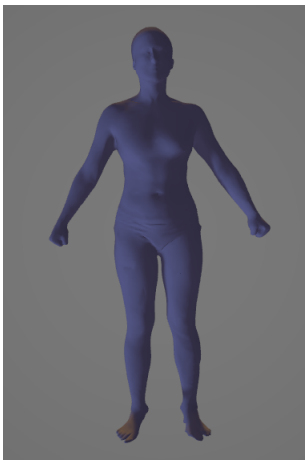

Figure 4.2: A mesh from the *Semantic Parametric Reshaping of Human Body Models* [4] results dataset that will be used to train our approach.

models, from the *CAESAR* dataset, which have been placed in point to point correspondence. Correspondence is established by nonrigid deformation of a template mesh obtained from averaging all female and male meshes (separately).

The semantic Parametric Reshaping is accomplished by using the *SCAPE* [44] model to learn the pose and shape deformation. After the transformation matrices of shape variation across different individuals are obtained, Yipin Yang introduced a regression model to explore the space of detailed semantic parameters. The pose is separated from the shape using transformation matrices for each triangle in each mesh, after this process the shape of each mesh can be obtained.

After the shapes of each mesh are obtained, Yipin Yang [4] uses a linear regression method to learn a linear mapping between semantic parameters (body measurements) and the model parameters. They used 23 semantic parameters, e.g., forearm length, neck height, head circumference, and shoulder breadth. The Local Mapping model is a linear regression model which directly learns a mapping between semantic parameters and shape deformation matrices. The template model has been segmented into 16 rigid parts beforehand and then the semantic parameters are binded to each part. For example, forearm length and circumference belong to the forearm part. Finally, they decide which semantic parameters influence the triangular faces using a function Φ. For a more detailed explanation, please refer to [4].

Point Correspondence

The *Semantic Parametric Reshaping of Human Body Models* dataset [4] is in point correspondence. It means that

for two meshes m_1 and m_2 all vertices $v_i \forall i$ in V are in the same semantic region.

An example is represented in Figure 4.3, where 2 completely different meshes are represented. In the image, m_1 is a female mesh with a more petite figure, while m_2 is a male mesh with a bigger constitutions. Both meshes have the vertex v_{3025} selected, represented by a blue number. Besides all the differences between m_1 and m_2, the vertex v_{3025} is on the shoulder in both. This allows an easier approach in later stages, specifically in the segmentation detailed in Section 4.1.3 and in the extraction of body measurements detailed in Section 4.1.4.

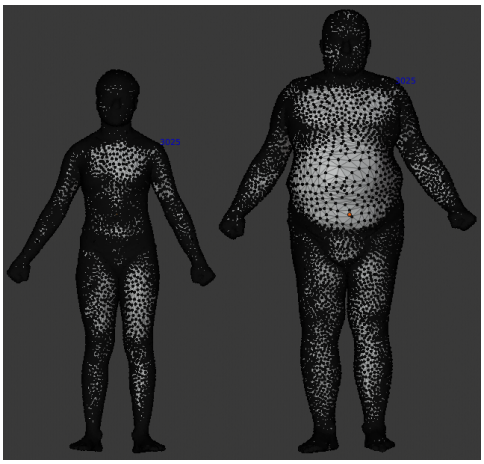

Figure 4.3: Point-to-point correspondence among different samples of the *Semantic Parametric Reshaping of Human Body Models* dataset [4]. Both samples vertex v_{3025} is located on the shoulder, despite the shape differences between the samples.

4.1.2 Mesh Repair

The *Semantic Parametric Reshaping of Human Body Models* [4] dataset was created by fitting a template mesh into the cloud points of the *CEASAR* dataset. This allowed all meshes to contain the same number of vertices, and for those vertices to be in point to point correspondence. However, the software that were used while producing [4] probably did not consider that the mesh contained non-manifold vertices.

We imported a random mesh of the dataset to *Blender*[1] software and an initial evaluation of the mesh showed that it required more fixing than expected. The mesh contained non-manifold vertices on the left foot, as you can see Figure 4.4, that that could become a problem in later stages as it could interfere with the extraction of body measurements. The figure shows 3 selected vertices $v_1 = 3070$ $v_2 = 3068$ and $v_3 = 3138$, and therefore 3 selected edges $e_1 = (v_1, v_2)$, $e_2 = (v_2, v_3)$ and $e_3 = (v_3, v_1)$. There are many reasons for a geometry to be classified as non-manifold, but in this case the edge e_1 is shared by more than 2 faces.

[1] https://www.blender.org/

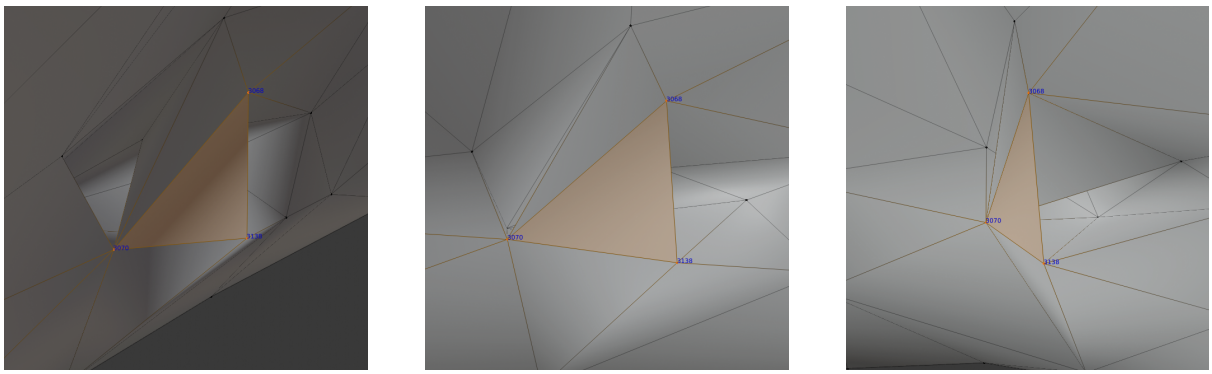

(a) Left view. **(b)** Front View. **(c)** Right view.

Figure 4.4: Nonmanifold vertices selected with *Blender* of a random mesh of the *Semantic Parametric Reshaping of Human Body Models* [4].

To solve this problem, it is necessary to repair all meshes of the dataset. Unfortunately, *Blender* is unable to do that, so we needed to use another software to repair the meshes. We used the *Wrap 3*, a paid tool of the company *Russian 3D Scanner*[2]. Wrap changes the way you process 3D-scan data. When working with a large set of similar objects like human scans, Wrap makes it possible to take an existing base mesh and non-rigidly fit it to each scan. It also provides a set of very useful scan processing tools like decimation, mesh filtering, texture projection, and many more. Another advantage is that it allows bulk changes, so it is possible to apply the same operation to all meshes in the dataset. Since this is a paid tool, we took advantage of the free trial to execute the repairing process.

Wrap 3 solved the non-manifold vertices by adding more vertices to where was an edge shared with more than 2 faces. In Figure 4.5, it is visible the result of the repairing process, the shape is maintained, but index of the vertex more to the left is not perceptible. This is because there is two indexes in the same spot, the initial vertex v_1 and the new added one $v_4 = 12489$. By adding v_4, a new edge $e_4 = (v_4, v_2)$ is created, and one of the 3 faces that were using e_1 is deleted and a new one is formed by using e_4 instead.

In the end, the repairing process added 5 more vertices to each mesh, resulting in a repaired dataset where each mesh contained 12505 vertices and no non-manifold vertices.

4.1.3 Segmentation

After the repair process, all meshes of the newly repaired dataset are ready to be segmented. This step is fundamental in the body measurements extraction phase. We performed segmentation in that all vertices are grouped in a body region. We used manual segmentation in a single mesh, no matter the gender, and replicated it to the

[2] https://www.russian3dscanner.com/

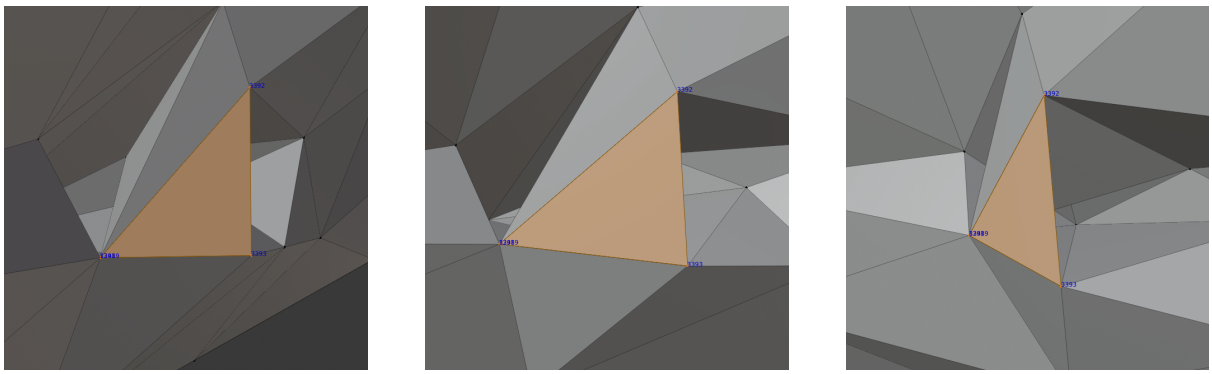

(a) Left view. **(b)** Front View. **(c)** Right view.

Figure 4.5: Nonmanifold vertices selected with *Blender* of a random mesh of the *Semantic Parametric Reshaping of Human Body Models* [4].

other meshes. This is possible due the point correspondence of the dataset. In first place, we manually grouped the desired vertices into 17 vertex groups using the *Blender* interface on a random mesh, and then we replicated the segmentation to the other meshes using a Python and Blender integration module - *blenderpy*[3] - for python. In Figure 4.6 is represented the segmentation result in two distinct meshes. From the figure, we see that the segmentation was well accomplished, because all body parts from both meshes are in equivalent places.

Figure 4.6: Segmentation result.

Some white bands are visible in the Figure 4.6, however that is not an alarming issue. This is happening because of the way the meshes were painted in *Blender*. In Figure 4.7 is represented a close-up of the border between the torso and the breasts of the mesh on the right on Figure 4.6. On this image, the vertices are also represented by a black dot, and it is visible that all vertices belong to one and only one color. Since we are

[3] https://pypi.org/project/bpy/

grouping vertices, and not faces, there will always be faces that have vertices that belong to different body parts (vertex groups), and that will result in white faces. However, since all vertices are in a vertex group, it is irrelevant if a face is painted or not. The Figure 4.6 was merely a visual guidance of the different segmented body parts.

Figure 4.7: Segmentation result.

At the end of this process, we had a new dataset regarding the body part that each vertex belongs to. In this specific one, there is no need to include information regarding the mesh, because all have the same vertex groups with the same vertices.

4.1.4 Extracting Body Measurements

Since the *Semantic Parametric Reshaping of Human Body Models* [4] dataset do not contain body measurements aggregated to the meshes, it is necessary to extract the measurements at the preprocessing stage. The measurements are used to learn the human shape variation and apply deformations on a template mesh to provide it a more realistic look according to the inserted measurements.

Users will manually insert body measurements as the system's input. The measurements required are split into three different categories: *girth* that measures the distance around the middle of something, *length* and *height* that measure the distance between 2 points. The extracted body measurements were tabled values that are mostly used by the fashion industry, and this measurements are represented in Tables 4.3, 4.2 and 4.1.

The point correspondence feature of our dataset becomes useful again to extract body measurements by defining the initial and target points of the distance to measure. The information regarding all initial and target points of all body measurements are saved in the form of a table, and since all meshes are in point correspondence, this information is equal to all meshes. For instance, let v_{10843} be the vertex that is in the top of the shoulder and v_{11830} a vertex that is on the wrist. The length of the arm is measured from the shoulder to the wrist, and in this case it can be measured by calculating the distance $D(v_{11830}, v_{10843})$. The arm length of all meshes can be calculated using the same formula thanks to the point correspondence feature. All points required to extract the measurements were predefined manually in one random mesh, and automatically applied to all meshes.

	Height	
	Measurement Parameter	**Definition**
7	*Waist to Knee*	The distance between the waist and the knee.
15	*Waist*	The distance between the waist and the floor.
17	*Inseam*	The distance between the lower groin point and the ankle.
27	*Feet*	The distance between the ankle and the floor.
31	*Torso*	The distance between the neck and the lowest groin point.
36	*Neck*	The distance between the jaw and the collarbone.
37	*Hips to Ankle*	The distance between the hip and the ankle.

Table 4.1: Height type measures asked as input by the system. Users will need to measure themselves, it might be required an extra person to help to take the measurements.

Height

One of the three measurement types are the *height* body measurements. Just as the name indicates, these measurements define the height of body components. For instance, the height of a person is defined by the difference of the top point of the person's head and the lower point of the feet. The height measurements list is defined on Table 4.1.

To calculate the difference between the points, we use the Euclidean distance, expressed in Equation 4.1. In this precise example, we calculate the distance between *a (0, 0, a_z)* and *b (0, 0, b_z)* to only calculate the distance regarding the *z* axis, the axis that defines height.

$$d(a,b) = \sqrt{\sum_{i=1}^{n} (b_i - a_i)^2} \tag{4.1}$$

Length

The second type of body measurements are the length measurements. These measurements consist on the distance between two points considering the mesh's surface that contains the initial and target points. This type of measurement is useful to calculate the distance between two body parts considering the body shape, just like fashion designers when extracting body measurements from models. The Table 4.2 contains the body measurements extracted using this type of measurement.

The computation of geodesic distances is the perfect way to simulate the work of a modiste or fashion designer, since it computes the distance between 2 points on a mesh considering its surface. In Figure 4.8 is an example of a geodesic line on a human 3D mesh, and it is visible that the line is on the surface of the mesh

	Length	
	Measurement Parameter	**Definition**
3	*Shoulders*	The distance between the shoulders following the collar bones.
5	*Rise*	The distance between the waist passing by the crotch to the back point of the waist.
16	*Glutes*	The distance between the back point of the abdomen passing by the center of the glute to the beginning of the leg.
17	*Neck to Waist*	The distance between the center back point of the end of the neck to the back center point of the waist.
18	*Collarbone to Waist*	The distance between the top point of the collarbone passing by the widest part of the bust to the waist.
20	*Upper Arm*	The distance between the shoulder to the elbow.
21	*Lower Arm*	The distance between the elbow to the wrist.
22	*Breast*	The distance between the top point of the chest passing by the widest part of the bust to the under bust.
25	*Front Lower Trunk*	The distance between the central point of the waist to the lowest point of the groin.
30	*Armpit to Waist*	The distance between the lowest point of the armhole to the waist.
31	*Collarbone to Under bust*	The distance between the collarbone passing by the widest part of the bust to the under bust.
32	*Under bust to Belly Button*	The distance between the central front point of the under bust to the belly button.
35	*Arm*	The distance between the shoulder passing by the elbow to the wrist.
37	*Groin*	The distance between the lowest central point of the abdomen to the lowest point of the groin.
38	*Belly*	The distance between the lowest central point of the under bust to the lowest central point of the abdomen.

Table 4.2: Length type measures asked as input by the system. Users will need to measure themselves, it might be required an extra person to help to take the measurements.

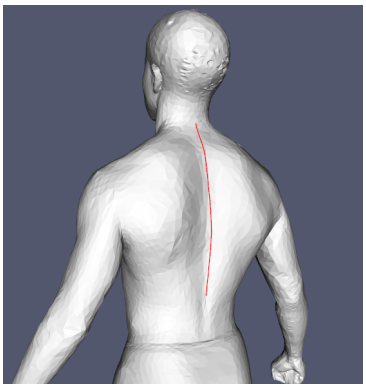

Figure 4.8: Geodesic line from the neck to the waist of a human body 3D mesh. This measurement can be helpful to produce clothing, like a t-shirt or even a shirt.

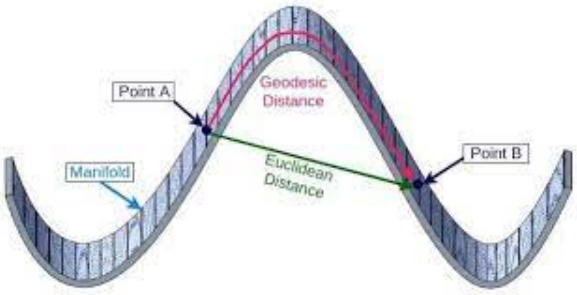

Figure 4.9: The comparison between geodesic and euclidean distances over a mesh's surface.

instead of intersecting it.

In Figure 4.9 is a better representation of the difference between the geodesic and euclidean distances. Both distances have the goal of measuring the distance between two distinct points, they just do it differently. The green line that represents the euclidean distance, calculates the distance between v_A and v_B directly in the 3D space, however the red line, representing the Geodesic Distance, goes from v_A to v_B by traveling on the mesh's surface. This process is similar to the Dijkstra search algorithm [52] for finding the shortest paths between nodes in a graph, where in this case the nodes are the mesh's vertices and the links are it's edges. The main difference between Dijkstra and the geodesic distance is that Dijkstra only travels node by node, where geodesics are able to intersect edges, allowing it to form paths that are straight lines. This particular feature of the geodesic distance is what elects it as the most useful distance to calculate the length measures of the dataset.

The easy, but inaccurate, way to compute the geodesic distance between two vertices of a triangle mesh surface is to run a shortest path algorithm on the mesh graph, where the weight associated with an edge is its length. Efficient algorithms, such as the Dijkstra [53], can compute these path lengths very efficiently, but can be shown to produce paths quite different from true geodesic paths. This is because the geodesic path does

	Girth	
	Measurement Parameter	**Definition**
1	*Waist*	The perimeter of the narrowest part of the torso.
2	*Head*	The perimeter of the widest part of the head.
4	*Bust*	The perimeter of the widest part of the bust.
6	*Hips*	The perimeter of the widest part of the hips.
8	*Knee*	The perimeter of the widest part of the knee.
9	*Ankle*	The perimeter of the narrowest part of the ankle.
11	*Neck*	The perimeter of the narrowest part of the neck.
12	*Lower Arm*	The perimeter of the widest part of the lower arm.
13	*Upper Arm*	The perimeter of the narrowest part of the upper arm.
14	*Wrist*	The perimeter of the narrowest part of the wrist.
16	*Tight*	The perimeter of the widest part of the tight.
18	*Calf*	The perimeter of the widest part of the calf.
22	*Arm loop Girth*	The perimeter of the loop from the top of the shoulder to the armpit.
26	*Elbow*	The perimeter of the widest part of the elbow.
29	*Abdomen*	The perimeter of the widest part of the abdomen.
30	*Under bust*	The perimeter of the widest part of the under bust.
32	*Mid Tight*	The perimeter of the narrowest part of the mid tight.

Table 4.3: Girth type measures asked as input by the system. Users will need to measure themselves, it might be required an extra person to help to take the measurements.

not necessarily pass through the mesh vertices, rather takes shortcuts through edges. D. Martinez, L. Velho, P.C. Carvalho proposed in 2004 an approach that computes a geodesic path over a triangulated mesh [54] that does precisely that. The result is an almost straight line on the surface of a mesh between two points. By using geodesic distances it is possible to measure the arm length or any other body measurements regarding length.

To calculate the geodesic distances, the python library *pygeodesic* [55] was used. This library computes geodesic distance over a triangular based surface mesh and is *Cython* wrapper of an implementation of the exact geodesic algorithm for triangular mesh first described by Mitchell, Mount and Papadimitriou in 1987 [56].

Girth

Girth measurements are calculated by intersecting a plane with the mesh to be measured. This is the only measurement type that does not take 2 points as input. It can either receive 3 or only 1. This measurement is quite close to the manual approach that modistes and fashion designers do. In Table 4.3 are represented the girth type body measurements.

This is also the more complex measurement that we dealt with. To extract someone's girth measurement using geometry, some complex calculations must be performed. The mesh's position and rotation must be

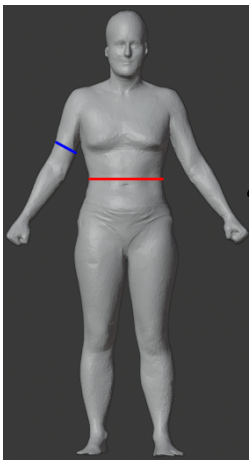

Figure 4.10: Different girth measurements, the red one represents the waist girth and the blue one the arm girth. The waist girth can be extracted in an horizontal plane, however we need to calculate the plane to extract the arm girth because it is not parallel to the ground.

considered in those calculations, and even if the mesh has a certain rotation, the arm might have another one. For instance, in Figure 4.10 is represented a mesh with a blue line on its arm and a red one on its waist. Each line represents a girth measure of that specific body part. We can see that with the exact pose that the mesh has, we can extract the waist girth on an horizontal plane, however to extract the arm one we need to calculate the rotation of the plane that we will extract the measure from. This happens because we won't manipulate the mesh's pose. We could pose the mesh with its arms perpendicular to the ground, what would allow us to extract the arm girth in an horizontal plane as well. But since this thesis do not consider the body pose, we do not manipulate the mesh's pose.

Intersection with Horizontal Constraints

In this thesis, we deal with girth measurements that can be extracted on an horizontal plane and measurements that can be in any possible plane. In this section, we will detail how we extracted the measurements that are under a horizontal constraint. In other words, we will explain how we extracted the measurements that are parallel to the ground.

As said in Section 4.1.4 that this measurement was the only one that did not have an initial and a target vertex, instead we can have 3 or only 1 point as input. Regarding measurements that are extracted under an horizontal plane, we only need 1 point as input. That point defines the height (z axis) where the horizontal plane must be positioned. This plane must be parallel to the ground and perpendicular to the mesh. In Figure 4.11 a is step by step visual representation of the process.

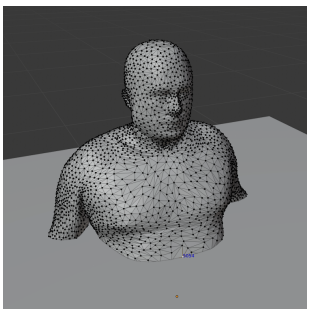

(a) An horizontal plane with v_{5054} as origin.

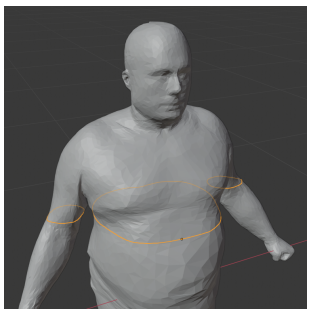

(b) The intersection between the mesh and the plane.

(c) Keeping only the vertices that are in the target zone to calculate the final distance.

Figure 4.11: Process of extracting the waist girth under an horizontal constraint of a random mesh. In *(a)* an horizontal plane is positioned on the scene, with the measurement's input vertex (v_{5054}) as origin. *(b)* we performed an intersection between the mesh and the plane, resulting in the yellow lines. (c) we then keep only the vertices that are in the area that we want to measure. The process of selecting the vertices that are on the correct body part is explained in Section 4.1.4. The last step of calculating the girth is to sum the size of all edges.

We first start by creating an horizontal plane with origin in the vertex received as input. In this specific case since we're calculating the waist girth, where the input vertex is v_{5054}. In Figure 4.11(a) you can see that v_{5054} is selected due the blue text, that means that the vertex with index 5054 is selected. After the plane is positioned in the right place, in this case it is positioned in the horizontal plane of the mesh's waist, an intersection between the mesh and the plane is performed. The result of that intersection can be visualized in Figure 4.11(b). However there is a problem, since we do not limit the plane's size, it intersects the entire mesh, not just the torso body part. To solve this problem we classify each new vertex resulting of the intersection to a certain body part defined by segmentation. That process is detailed in Section 4.1.4. Figure 4.11(c) shows the result after the classification process is complete. All new vertices are now assign to a body zone and we simply select the ones that belong to the torso, deleting the other ones. The final step is to sum the size of all edges that form the final ring around the mesh, that provides us the waist girth distance.

Intersection Without Constraints

The extraction method of a girth measurement without a horizontal constraint is pretty similar to the one described in Section 4.1.4, however there is a difference on how we calculate the plane location and rotation. In Figure 4.12 a is step by step visual representation of the process.

Lets say that our goal is to calculate the upper arm girth, where we define our input points as v_{3854}, v_{10985} and v_{11580}. We can create a new plane based on 3 points using an equation. The equation of a plane in 3D space can be written in algebraic notation as in Equation 4.2, where at least one of the real number constants a, b and

(a) A plane formed by v_{3854}, v_{10985} and v_{11580}.

(b) The intersection between the mesh and the plane.

(c) Keeping only the vertices that are in the target zone to calculate the final distance.

Figure 4.12: Process of extracting the upper arm girth giving 3 points as input on a random mesh. In *(a)* an plane is positioned on the scene, based on the measurement's input vertices (v_{3854}, v_{10985} and v_{11580}) as origin. *(b)* we performed an intersection between the mesh and the plane, resulting in the yellow lines. (c) we then keep only the vertices that are in the area that we want to measure. The process of selecting the vertices that are on the correct body part is explained in Section 4.1.4. The last step of calculating the girth is to sum the size of all edges.

c must not be zero, and x, y and z represent the axes of the three-dimensional plane. Since three points are given, we could determine the plane by using vector cross-products.

$$ax + by + cz = d \tag{4.2}$$

To extract the upper arm girth, we first define a plane using v_{3854}, v_{10985} and v_{11580}. In Figure 4.12(a) you can see that v_{3854}, v_{10985} and v_{11580} are selected. After the plane is positioned in the right place, an intersection between the mesh and the plane is performed. The result of that intersection can be visualized in Figure 4.12(b). However, we still have the same problem of being able to select the right vertices to consider in our measurement.

Classifying New Vertices

Our strategy uses a classifier to group the new vertices, resulting from the intersection of the plane with the mesh, to the correspondent body parts represented in Figure 4.6. The classifier is a K-Nearest Neighbors (KNN), and it considers the mesh's vertex groups represented in Figure 4.6 and the mesh's vertices to classify a new vertex. The classification is trained with the mesh's vertex indices as the training dataset, and the information regarding the body part to what each vertex belongs to as target classes. Right after the intersection, several new vertices are added to the scene like shown in Figure 4.13(a), this new vertices at that stage do not belong to any body part. However, after training the *KNN* classifier, all new vertices will be inserted in the model and the new

assigned class (body part) will result from it.

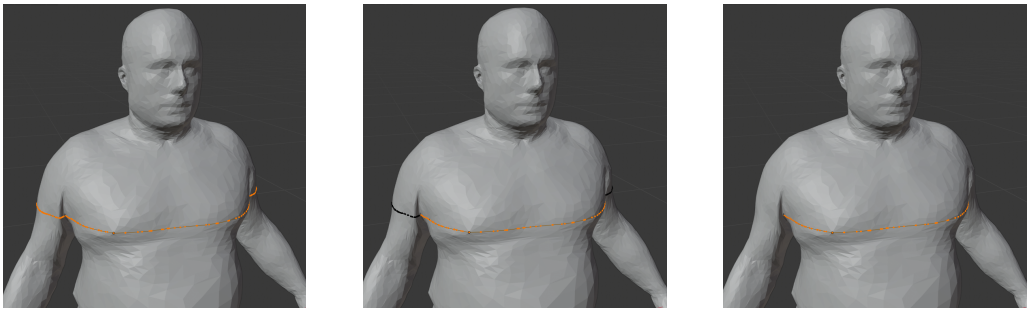

(a) An horizontal plane at breast height.

(b) Selecting the vertices that belong to the torso.

(c) Deleting the unnecessary vertices.

Figure 4.13: Process of extracting the bust girth on a larger mesh. In *(a)* an plane is positioned on the scene, based on the measurement's input vertices (v_{4873}) as origin. In the figure is represented the intersection result of the mesh with the plane. *(b)* we classify each new vertex resulting from the intersection as being part of a certain body part represented in Figure 4.6 using *KNN*. Only the vertices that belong to the torso and breasts are selected. (c) we then delete the vertices that are not selected.

The way the *KNN* works is through distances relatively to the closest vertices of the classifier. Since that we trained this classifier with information that we obtained from the segmentation process, explained in Section 4.1.3, for each new vertex, the euclidean distance to all classified mesh's vertices will be calculated. After all distances are calculated, the K-nearest vertices are selected and the final class will be the one that is in majority. It is important for K to be an odd number to avoid ties, in this thesis we classified the vertices with K=5. Let a vertex v_i be closest to other 5 vertices that belong to the torso, it means that v_i will also be classified as being part of the torso. In other case, if v_i is closest to 3 vertices that belong to the breast and 2 that belong to the torso, it means that v_i will belong to the torso. When all new vertices are classified, the result is exemplified in Figure 4.13(c), all vertices that belong to the body part that is being measured are selected, while the ones that do not belong to the target body part are deleted.

The classification process does not solve the body parts union, represented in Figure 4.13(a). In the bust girth extraction process, the result after the classification are two lines that are not connected, an example is represented in Figure 5.6. In here we can see that if we sum the size of all edges, the final measurement would be much smaller than the real one.

To solve the problem of the resulting vertices not being connected, a simple strategy is used: for each vertex that is only connected to one edge (there will be four in total), the closest vertex that is also connected to only one edge will be calculated. From this, it will return two unique combinations, where the distance between the vertices that compose those two combinations will be added to the resulting value of the intersection repre-

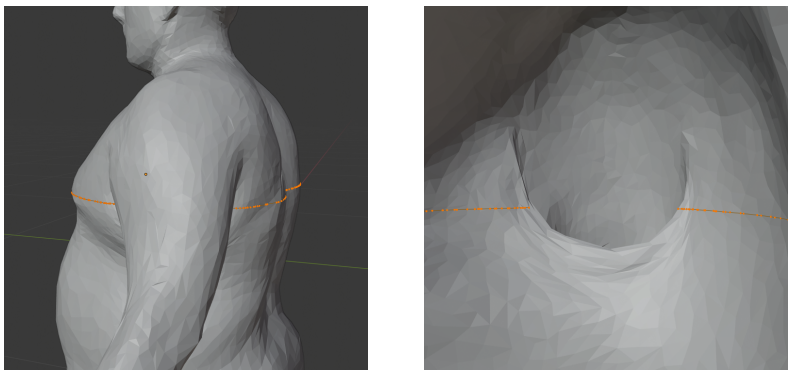

(a) External mesh view. **(b)** Internal mesh view.

Figure 4.14: The result of the classification process when extracting the bust girth. In *(a)* the resulting line of the intersection does not include the arm like in Figure 4.13(a) anymore, resulting in a "hole" that is more visible in *(b)* from the interior of the mesh.

sented in Figure 4.13. The combination of the *KNN* classifier and the approximation distance of the unlinked components returns a value that is very close to the method used by modistes and stylists.

4.1.5 Building Three new Datasets

At the end of the preprocessing module, four datasets are created from extracting information of the *Semantic Parametric Reshaping of Human Body Models* [4] original dataset. These datasets contain information about the meshes vertex coordinates, the body measurements of each mesh, the 17 different body parts and what vertices belong to each one, and finally the dataset with the required vertices to extract the body measurements. Only the first and second one will be used in the model generation module, in order to relate the body measurements with the human shape variation.

Saving Coordinates

Right after the repair process, detailed in Section 4.1.2, is complete we extract the vertex coordinates of all meshes to an excel sheet. The format of the table is represented in Table 4.4 with only two meshes as an example (rows). It is visible that the table has an header composed of three different information regarding the vertices. The first line of the header corresponds to the body part that that vertex belongs to, the second line corresponds to the index, and the third corresponds to the axis. The columns are organized in order that each vertex information is grouped in three different columns. This way, we get a table that as 3x as many vertices that the meshes have, resulting in $3 \times 12505 = 37,515$ columns. This table will then be used to calculate both

models detailed in Section 4.2.

	Left Hand			Left Hand			Left Hand			...	Groin		
	0			1			2				12504		
	x	y	z	x	y	z	x	y	z		x	y	z
1	0.34	-0.27	-0.15	0.34	-0.26	-0.15	0.34	-0.27	-0.14		-0.04	0.05	-0.25
2	0.32	-0.24	-0.17	0.32	-0.24	-0.17	0.32	-0.24	-0.16		0.00	0.02	-0.25

Table 4.4: Sample of the table containing the coordinates information of all meshes.

Saving Measurements

The second dataset that will also be used in the next stage is the one that contains information regarding the body measurements. This table is simpler than the one described in Section 4.1.5, however it is not less important. This table only considers the body measurement names and their values for the meshes. In Table 4.5 is represented a sample of the table. Each row represents a distinct mesh with several body measurements. Since one of the goals of this thesis is to discover the principal measurements to describe a human body shape, several body measurements were extracted in order to compare all of them and decide what are the more relevant ones.

Mesh	Waist Girth	Head Girth	Shoulder Length	Bust Girth	Rise Length	Hips Girth
1	0.79	0.53	0.11	0.92	0.82	1.06
2	0.87	0.60	0.13	1.23	0.74	0.96

Table 4.5: of the body measurements table where each row corresponds to a shape and each column a measurement.

4.2 Model Generation

The preprocessing phase results in a clean selected dataset that can be used to fuel our model to generate new body shapes entirely from a set of body measurements. In this section, we explain how we generate new body shapes from a set of body measurements.

We compare two distinct methodologies against each other, the first simply uses linear transformations to output a new body shape, while the second one uses feature extraction to explain the maximum variance in the human body. However, before we estimate any new body shape, it is fundamental to decrease the number of features that the dataset contains. To fulfill our goal of obtaining the minimum body measurements set that explains as much information as the original set as possible, we perform unsupervised feature selection on the original dataset. In this thesis, we do not want to classify the gender of a mesh, or the age, we do not have a classification problem in hand. Thus, the usage of supervised methodologies for body measurement selection

would be ineffective for this thesis. The process of feature selection reduces the used features to approximately 17%, resulting in only seven final features of the initial 41. Both of our models use the subset returned from the feature selection process to output new body shapes.

We describe in detail the process of feature selection in Section 4.2.1. The explanations of both our models are explained in Sections 4.2.3 and 4.2.2. Both of this models will be tested on several body measurement subsets, including the one returning from the feature selection process. The results can be seen in Chapter 5.

4.2.1 Feature Selection

We first start by selecting the minimum number of features that explain the maximum of the human body variance. We perform feature selection strategies on the original body measurements dataset returned from the Section 4.1.5, in order to reduce the number of features required to output a new realistic body shape.

The idea is to have the minimum number of measures as possible to achieve maximum accuracy. There are several feature selection strategies, all of them with the goal of reducing the number of variables used. However, feature selection is highly dependent on the dataset, and its characteristics. In this thesis, we want to study the human body shape variation and relate that variation with the body measurements. This problem is not a classification problem because we do not want to classify a body shape, or gender, or anything, we do not have a target class. That means that observing the human shape is an unsupervised problem and requires an unsupervised feature selection approach. For this thesis we filter the more important variables by their variance and correlation.

The usage of the variance in the selection of variables is important because we want to keep the variables that describe better the body shape variation. Let S be a set of meshes and $d_{waist\_girth}(s) = 0.5cm \forall s \in S$. In this particular case, $d_{waist\_girth}(s)$ would not be a good choice because it would describe all shapes the same way, the variance ($v(d_{waist\_girth}(s))$) would be 0 and it would add redundant information to the subset. When we are performing feature selection and find a variable with a lower or no variation at all, we exclude that variable, thus $d_{waist\_girth}(s)$ would be filtered and would not be present in the final subset resulting from the feature selection. Now if $d_{height}(s)$ was different for all meshes s in the *Semantic Parametric Reshaping of Human Body Models* [4], this measurement would be a good candidate to keep, especially if the values were very different among the meshes, or in other words, if it had a high variance.

Correlation is a powerful tool in feature selection as well, as it helps to filter variables that might add redundancy to the final subset. In statistics, correlation is any statistical relationship between two random variables.

In the broadest sense correlation is any statistical association, although it commonly refers to the degree to which a pair of variables are linearly related. This means that if $d_{waist\_girth}(s)$ and $d_{height}(s)$ are correlated, we can predict $d_{waist\_girth}(s)$ from $d_{height}(s)$ and vice versa. In addition, we can select only one measurement to the final subset while adding both would increase the redundancy. Therefore, we used correlation to minimize the number of body measurements used in the final subset by maintaining the ones that have no correlation with the others.

The usage of feature selection strategies were performed on male and female datasets separately. By doing this, we not only observed how the human body shape varies but also how gender impacts the human body shape. In the Section 4.2.1 we explain what was the process of analyzing the data to form the final subset that we used to test the models with real people, detailed in Section 5.3.2.

Data Analysis

The process of unsupervised Feature Selection consists on analyzing the data that we want to reduce. Therefore, since we want to filter the maximum body measurements as we can, we need to analyze the body measurement dataset obtained from Section 4.1.5 and that is the process we explain in this section. After obtaining the body measurements of several meshes present in the dataset, as explained in Section 4.1.4, it was required to analyze the results. Since the body measurements were obtained by directly measuring the dataset 3D models, they can be slightly different from the real body measurements of the scanned people that originated the dataset.

We analyzed the data separately by two genders: male and female. This way, we are able to see what are the body measurements that most affect both genders, and if there is any equality on how the body measurements affect human shape, independently of gender. Even though we analyzed both datasets separately in this document we focused our explanation more in the female one. Analyzing data is a long and complex process that involves a lot of plots and data visualization, and since the process is essentially the same for both datasets, we decided to explain the process with only the images regarding the female dataset in the main document. We will not ignore the results provided by the male dataset, we will simply explain the process with only one dataset for simplicity and to be easy to understand the process. All plots regarding the female dataset will be presented in this section, while the male ones are represented in Appendix A.

The first step was to analyze if are there any missing values for the measurements, however all measurements were filled for both genders. Since there was no missing data in the dataset, we could proceed by checking the distribution of each variable. The observation of the distribution of the variables was useful to spot any outliers in the data. An outlier is an observation that deviates significantly from the rest of the object collection, it might be an abnormality, and if so, it can add entropy to the model. The distribution regarding the female dataset is

represented in the Figure 4.15 while the distribution regarding the male body measurements is in Figure A.1(a). In this figure, all we can see how the variables differ from each other, for instance, the waist girth had a bigger variance than the head girth, it makes sense because human waists are wider than heads, and the variance of its value is higher. Let m_1 and m_2 be two female meshes, m_1 has a more petite figure with a thinner waist hips and bust while m_2 is way larger. In this specific case, the variance of the waist, bust and hips between m_1 and m_2 is higher than the variance of the head girth that probably will not change much. In Figures 4.15 and A.1(a), that was visible as well, compared to the waist, bust, and hips, the head girth had a smaller variance interval. Besides the variance interval represented by a box with two vertical lines (one on the top and one on the bottom), there were also visible dots above and below the intervals. These dots represent outliers, and almost every variable contains at least one. In Figure 4.15, the variable under-bust girth had an average of approximately *0.70m*, however there is a sample that measures *1.80m*. This value is almost impossible to reach, thus keeping it would have a negative impact on the model results. Overall, the under-bust and bust girths were the measurements with a higher number of outliers.

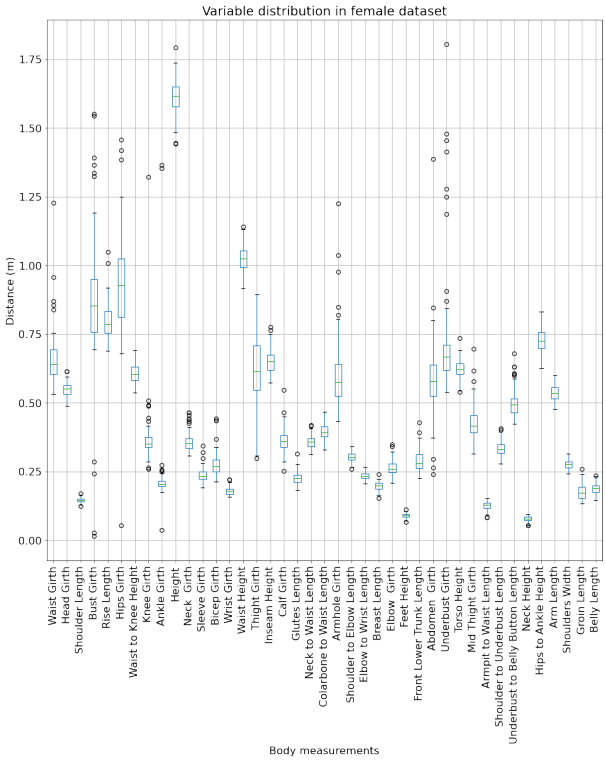

Figure 4.15: Distribution of the female body measurements.

Throughout the entire thesis work, these measurements proved to be the more challenging ones due the mesh position. The fact that the meshes are not in T-pose while extracting the body measurements, it creates a series of problems as explained in Section 4.1.4. Even with the vertex classification explained in Section 4.1.4,

errors occur and vertices might be mislabeled. A reason for the bust and under-bust girths to have so many outliers is because the arms are close to the torso, and in some cases, the horizontal planes in those measurements include the arms as well. The same happens in the tight girth, sometimes the plane can be positioned in a place that connects the groin and both legs, resulting in a bigger distance. Therefore, for all measurements, we excluded all values that were outside of the $\mu \pm 3\sigma$ Gaussian boundary, resulting in missing values instead of outliers. The plots that represent the count of missing values after we replaced the outliers by missing values are shown in Figure 4.16 and the distribution of the variables after removing the outliers is represented in Figure A.4(b). The count of missing values before excluding the outliers was zero for all measurements, something that do not apply after exclusion. Instead of removing the outliers, we could have applied another technique that consisted on replacing the outliers value by the mean or even the most concurrent value. However, the usage of this technique would change the measurements assigned to the meshes, and they would not be in sync anymore. If a larger mesh contained a bust girth that was considered an outlier and the bust girth value was replaced by a smaller value in the dataset, an average bust girth size would be assigned to a larger mesh. This would impact the results, especially when trying to reproduce a mesh with larger dimensions.

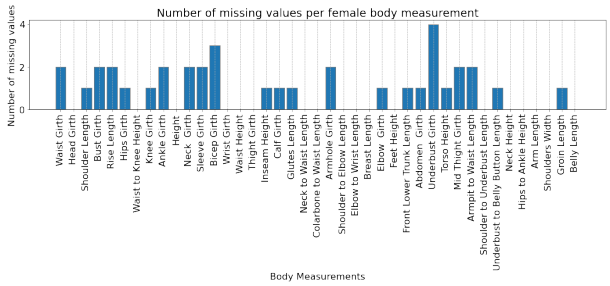

Figure 4.16: Missing values count after replacing all outliers by missing values.

In the image, we observed that some measurements have a higher number of missing points than others. The underbust girth measurement pops out for the one with a higher value, followed by the bicep girth. In the case of the male database, the armhole girth is the measurement with a higher number of missing values followed by knee girth. It is important to notice that the higher values in both Figures 4.16 and A.3 are related to the higher variance in Figures 4.15 and A.1(a), respectively, because the outliers that increased the variance in Figures 4.16 and A.3 were the missing values represented in Figures 4.15 and A.1(a). We decided to exclude the samples that have a higher number of outliers. Deleting the columns that have a higher number of outliers: underbust, bicep, armhole and knee girths in both datasets, was acceptable too, but since we want to see how the measures relate between each other we rather exclude the samples with outliers. After excluding the samples with outliers defined by being outside of the $\mu \pm 3\sigma$ Gaussian boundary, we can sort all variables by their variance and plot it. In Figure 4.17 is represented the plot with the sorted variance.

We represented the variables sorted by their raw variance in Figure 4.17(a), and by their normalized variance in Figure 4.17(b). To select the final subset of variables, we selected the ones that have a higher variance. This strategy is unsupervised, because we did not contain a target variable in the dataset. By observing the Figures 4.17(a) and 4.17(b) it was possible to see that there are some differences between them. In Figure 4.17(a) the variance values are higher overall, with the bust girth reaching approximately 0.62cm while in Figure 4.17(b) it reaches 0.42cm. The variables sequence is different, the second body measurement with a higher variance in 4.17(a) is hips girth with almost 0.6cm of variance, while the second body measurement in Figure 4.17(b) is ankle girth with almost 0.4cm, followed by hips girth with almost 0.6cm of variance.

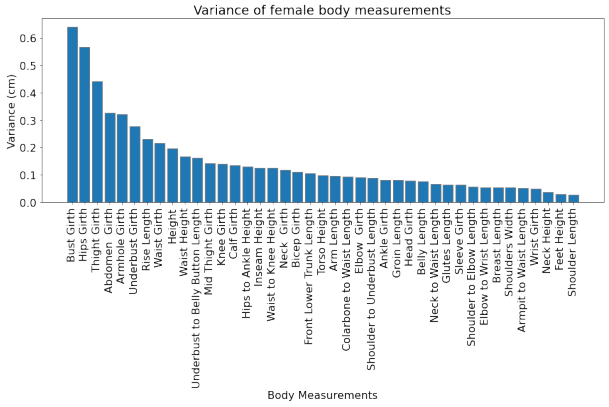

(a) Female body measurements sorted by their raw variance.

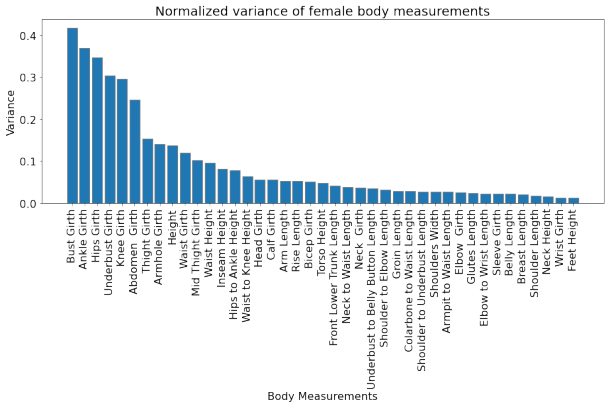

(b) Female body measurements sorted by their normalized variance.

Figure 4.17: Female body measurements sorted by their *(a)* raw variance and *(b)* normalized distance.

There is a reason for Figures 4.17(a) and 4.17(b) present different values and sequences even if they represent the same information. In Figure 4.17(a) is represented the raw values of each measurement variance, by other

words, it is represented the absolute value of the difference between the minimum and the maximum of each variable. This pushes the measurements that naturally have a higher variation to the top, like bust, abdomen, hips, girth and height, while the body measurements that naturally have a low variance like neck height and elbow girth are pushed to the bottom of the list. Even that the Figure 4.17(a) shows a lot of information regarding how the variables vary, it is not a good idea to decide our final subset from this plot. In Figure 4.17(b) the variables were normalized before they were sorted. This means that each variable was scaled by shifting their values so that they end up ranging between zero and one. This process brings equality to all measurements by being able to directly compare the height with the head girth and see which one changes more overall. However, we excluded the outliers that were outside the $\mu \pm 3\sigma$ Gaussian boundary. Inside of that boundary we still have outliers as it is visible in Figure A.4(b), what impacts the variance in Figure 4.17. For instance, ankle girth is in the second place because it has a single outlier that is very separated from the other values, the same applies to underbust girth, knee girth and armhole girth.

If we select the top ten body measurements that most vary in the female dataset, the list would be: bust, ankle, hips, underbust, knee, abdomen, thigh and armhole girths, height and waist girth, however, this list contains variables that have a high number of outliers. If we remove the variables with a higher number of outliers (by observing Figures 4.16 and A.3), the top ten female body measurements became: bust, hips, abdomen and thigh girths, height, waist, mid-thigh girths, waist inseam and hips to ankle height, while the male one became: bust, hips and thigh girths, rise length, waist and abdomen girths, height, underbust to belly button length, neck girth and waist height. There were many measurements that both genders shared, while there are others that were characteristic of each gender. For instance, the neck girth varies much more among males than females, while the mid thighs vary much more among females than males. Selecting ten variables out of 41 is already a reduction of more than 83% of the original dataset, but we can reduce the final subset even more.

It is interesting to notice that the female body measurements that vary the most are the ones that affect the lower part of the body, while in the males it is exactly the opposite. According to this result, females vary more on the lower part of the body while males vary more on the upper part of the body. To further decrease the final subset, we analyzed the relation between the variables, something that was accomplished by calculating the correlation between the variables. In Figures A.5(b) is represented the correlation matrix of the female body measurements. The correspondent matrix for the male body measurements is represented in Figure A.5(a). In both figures, there is a correlation scale that goes from -1 to 1. The minimum possible value for correlation (-1) does not mean that the two variables are not correlated at all, but it means that they are inverse correlated. An inverse correlation is a relationship between two variables such that when one variable is high, the other is low and vice versa. This way, all squares that are blue or red define a correlation relationship, only the whiter ones determine the nonexistence of a correlation relationship. Using this relationship, we can exclude measurements

from the top 10 that have a high correlation among them. For better interpretation of the results, the correlation between only the top ten measurements with the female measurements is represented in Figure 4.18, while the male is represented in Figure 4.19.

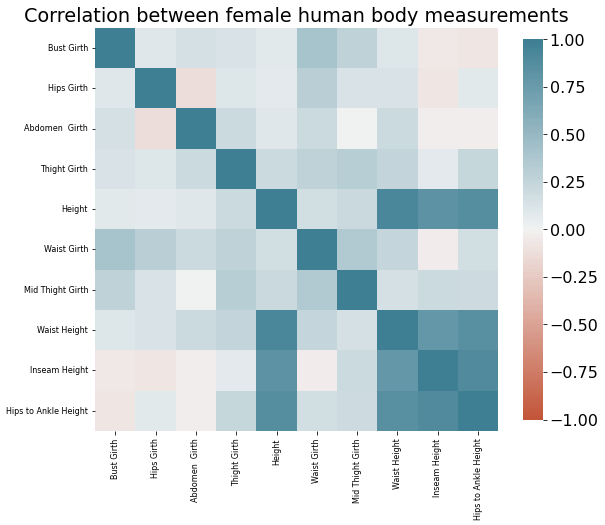

Figure 4.18: Correlation of the top 10 female body measurements.

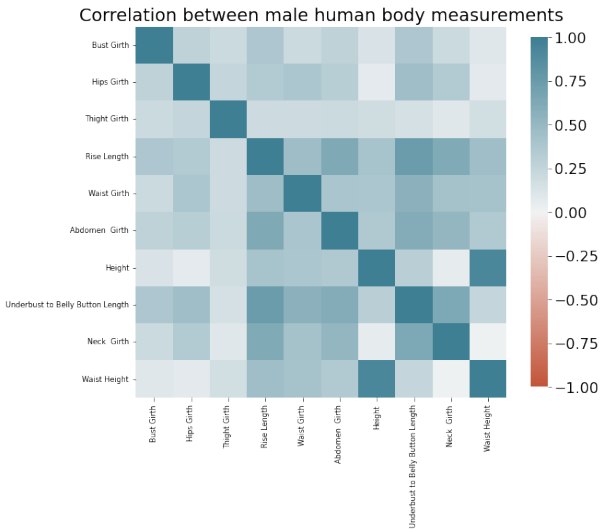

Figure 4.19: Correlation of the top 10 male body measurements.

In both genders, all height measurements were highly correlated. In Figures 4.18 and 4.19 we can see that in the height row, the bluest squares are the ones that are also other height measurements: waist to knee height, waist height, inseam height and hips to ankle height. This means that all these measurements can be predicted using only the height measurement. Thus, any other height measurement in the top ten, besides height, can be removed without any information loss. Consequently, the measurements subset for the female dataset is

composed by bust, hips, abdomen and thigh girths, height, waist and mid-thigh girths, while the male one is composed by bust, hips and thigh girths, rise length, waist and abdomen girths, height, underbust to belly button length and neck girth. By removing all height measurement, besides the height itself, from the top measurements, the female subset gets with seven measurements and the male one with nine. Both subsets have height and bust, hips, thigh, waist, and abdomen girths in common, which are exactly the set of measurements that most systems ask for. In the male dataset, the neck girth is correlated both with the rise and underbust to belly button lengths. This means that the neck girth contains a high percentage of the information that those two measurements contain, and if we delete them, we would still have partial information about them in the neck girth measurement. Thus, we removed them and the top male measurements are now the height and bust, hips, thigh, waist, abdomen, and neck girths. After removing these two measurement of the male subset, we have only two measurements that are not present in both subsets: the neck girth is only present in the male subset and the mid-thigh girth is only present in the female one. However, those measurements are not correlated with the other 6 measurements of the subset and need to be kept there.

At the end of the feature selection process, we ended with two subsets of seven body measurements for both males and females. Both subsets share six measurements in common, leaving only one measurement that is unique for each gender: neck girth for males and mid-thigh girth for females. We were able to reduce the initial set of measurements by almost 83%.

Selected Body Measurements

The final subsets are represented in Table 4.7. The table is sorted from a higher (1) to lower (7) variance and the first six elements of both subsets are common in both, only the last element of each subset is unique: mid-thigh girth for the female subset and neck girth for the male one. This is interesting because it shows us that the measurements that best describe the human shape are essentially the same for both genders.

At the end of the feature selection process, we ended with two subsets of seven body measurements for both males and females. Neither body measurement had a correlation relationship with other measurement of the subset, which means that the subsets do not contain redundant information. We were able to reduce the initial set of measurements by almost 83%.

Body Measurements	***Gender***	
	Male	*Female*
1	Bust Girth	Bust Girth
2	Hips Girth	Hips Girth
3	Thigh Girth	Abdomen Girth
4	Rise Length	Thigh Girth
5	Waist Girth	Height
6	Abdomen Girth	Waist Girth
7	Height	Mid-Thigh Girth
8	Underbust to Belly Button Length	Waist Height
9	Neck Girth	Inseam Height
10	Waist Height	Hips to Ankle Height

Table 4.6: Top 10 body measurements subset per gender sorted by higher (1) to lower (7) variance. Both subsets have 6 elements in common, but with a different variance level.

Body Measurements	***Gender***	
	Male	*Female*
1	Bust Girth	Bust Girth
2	Hips Girth	Hips Girth
3	Thigh Girth	Abdomen Girth
4	Waist Girth	Thigh Girth
5	Abdomen Girth	Height
6	Height	Waist Girth
7	Neck Girth	Mid-Thigh Girth

Table 4.7: Final body measurements subset per gender sorted by higher (1) to lower (7) variance. Both subsets have the first 6 elements in common (even with a different sequence) and only the last element of both subsets is unique.

4.2.2 Estimating New Body Shapes Using Feature Extraction

In this section, we explain the implementation of one of the two models compared in this thesis. This particular model will use feature extraction to understand how the human shape dataset, that returns from the Section 4.1.5, varies.

It is important to understand that the feature extraction process was be performed on a different dataset that suffered from the feature selection process. The feature selection was applied on the dataset containing the body measurements, while the feature extraction was performed on the dataset containing the vertex positions of the samples. This means that the feature extraction process is completely independent of the feature selection process. However, in this specific model, we used both processes. The feature extraction was performed on the coordinates dataset using Principal Component Analysis (*PCA*). This results in the model learning the principal components of the dataset. These principal components represent how the human shape varies the most, with each component representing a specific body variation e.g, the height, the breast size, the body volume, etc. These principal components were mapped as weights and are associated with the vertices of a template mesh obtained from the mean of the samples used to train our model. The template model was deformed by adding the weights associated with the new set of body measurements. Finally, once we inserted a new set of body measurements, the model outputted a new body shape that respected the body measurements inserted.

Template Shapes

The first step of this model is to calculate the template models for male and female genders. These templates consist on the mean of all male and female meshes in the dataset, respectively. It was of the most importance to calculate the template meshes because it was be the foundation of this model. Since this model uses only weights to calculate a shape, it is fundamental to relate those weights to something. The final mesh was the template mesh with the weights associated to the inserted set of body measurements.

Feature Extraction Algorithm

In this section, we describe one of the approaches that we used to deform 3D meshes based on body measurements. This approach was accomplished by extracting information regarding the vertex coordinates of the samples and is based on S. Wuhrer proposal for estimating human shapes based of body measurements [57]. As input to the method, it was given a database of n triangular manifold meshes S_0,..., S_{n-1} of human bodies with similar posture and a set of measurements P. Let P_i denote the measurements corresponding to S_i. Furthermore, we are given a set of distances P_{new}. Our aim is to estimate a shape S_{new} that interpolates the distances P_{new}. This approach proceeds by learning the correlation between the shapes and the measurements. When predicting

a new shape, this approach finds a solution based on the learned correlation.

We now consider learning a correlation between the set of shapes S_i and the corresponding measurements P_i. Since the database is parameterized - in point-to-point correspondence - the vertices and body parts can be given in terms of their vertex and triangle numbers on the mesh. In [57], S. Wuhrer implemented a model that learns a mapping between S and the space of human body shapes using feature analysis. This model was chosen because it describes both the shape space of S_i and the mapping from the space of measurements to the learned shape space using linear functions.

This approach consists on mapping the body measurements to the differences that they apply on the body, therefore two template meshes are used - one for each gender. The production of the template mesh $\bar{S}$ is explained in Section 4.2.2, and they are used to calculate how much the samples differ from it. Therefore, there is a new dataset D that is composed by the differences between all samples of S and $\bar{S}$, as it is demonstrated in Equation 4.3.

$$D = S_i - \bar{S}, \forall S_i \in S \tag{4.3}$$

The new dataset D is the foundation of this algorithm. From it, we can extract the principal components that make a human body vary, relate that variation to body measurements and create new shapes from an entirely new set of body measurements. Let D be a $(3v \times n)$ matrix, by performing PCA in D, it yields a matrix y that corresponds to the transformed dataset D and a matrix A that is a transformation matrix. The first matrix W and matrix D are the representation of the same information but in different spaces. By applying PCA to D we extract the information in the dataset by creating a new coordinates system that fits the data where it varies the most. In other words, we lose information regarding the variables of D because new ones are created. The second matrix A is the matrix that allows the transformation of D into W and vice versa, it is a transformation function. Thus, a new shape S_{new} can be estimated using the Equation 4.4 where the sum of the template mesh $\bar{S}$ and the weights of a new set of measurements W_{new} transformed by A result in a new shape S_{new}.

$$X_{new} = AW_{new} + \mu \tag{4.4}$$

However we still need to calculate matrices A and W_{new}. We know that W is D transformed into the PCA coordinate system, thus a transformation A is responsible for the coordinate system swapping. So, W is the result of the multiplication of A and D, what means that we can obtain A by multiplying W and D, like demonstrated in Equation 4.5 with D^+ being the pseudo-inverse of D.

$$W = AD \Leftrightarrow WD^{+} = ADD^{+} \Leftrightarrow WD^{+} = AI \Leftrightarrow A = WD^{+} \tag{4.5}$$

To calculate the weights matrix W_{new}, we need to take into consideration the body measurements and relate them to the PCA weight W_i of each mesh S_i. For that, we learn a linear mapping from P_i to W_i with $i = 0, ..., n-1$, by transforming each P_i to a new coordinate system W_i. To perform this, we need another transformation matrix B that maps body measurements to its corresponding PCA weight. We can infer B by assuming that W_i is the result of the multiplication between B and P_i, like demonstrated in Equation 4.6, with P^{+} being the pseudo-inverse of P.

$$W = BP \Leftrightarrow WP^{+} = BPP^{+} \Leftrightarrow WP^{+} = BI \Leftrightarrow B = WP^{+} \tag{4.6}$$

With this, we were able to relate the body measurements to the information extracted from the human body variation through PCA and give it a weight. It is important to notice that to reproduce the results obtained in [57] we must normalize each entry of W by its correspondent PCA eigenvalue. Finally, to estimate a new shape X_{new} based on a new set of body measurements P_{new}, we can transform P_{new} to the PCA coordinates, resulting in a weight vector W_{new} and then transforming W_{new} to the coordinate system that dictates the shapes. Therefore, we can re-write the Equation 4.4 into Equation 4.7.

$$X_{new} = ABP_{new} + \mu \tag{4.7}$$

The mapping between the measurements and the PCA weights of the 3D shapes learned allows us to find an new shape S_{new} new given P_{new}. With this process we can understand how much the human shapes vary from the average human shape $\bar{S}$. We can relate that variation with the body measurements P and estimate new shapes S_{new} with a new set of body measurements P_{new}. By adding the weights corresponding to a new set of body measurements W_{new} to the template mesh $\bar{S}$ we obtain a new shape that respects the variation dictated by P_{new}.

4.2.3 Estimating New Body Shapes Using Linear Transformations

In this section, we explain the implementation of one of the two models compared in this thesis. This particular model will use linear transformations that maps directly the coordinate dataset, explained in Section 4.1.5, with the body measurement dataset, represented in Section 4.1.5.

The second approach that we tried was to obtain a shape directly from the body measurements of Table 4.5. We accomplish this by creating a transformation matrix between the Tables 4.5 and 4.4. This way, we can easily transform a body measures vector into a coordinates vector without intermediate steps.

Linear Transformation Algorithm

In this section, we will describe one of the approaches that we used to deform 3D meshes based on body measurements. This approach is accomplished by using a linear map between the body measurements and the mesh's coordinates. In linear algebra, a linear map is a mapping $V \rightarrow W$ between two vector spaces that preserves the operations of vector addition and scalar multiplication. A linear map from V to W always maps the origin of V to the origin of W. Moreover, it maps linear subspaces in V onto linear subspaces in W (possibly of lower dimension). For instance, it maps a plane through the origin in V to either a plane through the origin in W, a line through the origin in W, or just the origin in W. Linear maps can often be represented as matrices, and simple examples include rotation and reflection linear transformations. This approach consists in defining a transformation matrix that maps a vector of body measurements into a vector of coordinates. The usage of matrices is useful because it allows concrete calculations.

Let S be shapes dataset that results from the process explained in Section 4.1.5 and M be the body measurements dataset resulting from Section 4.1.5. Both datasets contain k samples, because they both have different information regarding the same 3D objects. Each sample contains $3v$ vertices and m body measurements. The goal of the thesis is to convert body measurements into a 3D shape, thus we need to create a function T that maps a vector of body measurements M into a vector of vertices coordinates V, as shown in Equation 4.8.

$$T : M \rightarrow V \tag{4.8}$$

In this case, T represents a linear transformation mapping the space of body measurements to the space of 3D coordinates. So, T is a linear transformation mapping $\Re^m \rightarrow \Re^{3v}$ and given a column vector x with m entries then the transformation function can be represented as in Equation 4.9, where $T(x)$ returns a column vector with $3v$ elements.

$$T(x) = Ax \tag{4.9}$$

For $T(x)$ return a column vector with $3v$ elements, A must be a $(3v \times m)$ matrix. Note that A have $3v$ rows and m columns, whereas the transformation T is from $\Re^m$ to $\Re^{3v}$. This follows the linear algebra rule that for matrix multiplication to happen, the number of columns in the first matrix must be equal to the number of rows in the

second matrix. The resulting matrix has the number of rows of the first and the number of columns of the second matrix. With A being a $(3v \times m)$ matrix and x being a $(m \times 1)$ vector, the Ax multiplication results in a $(3v \times 1)$ matrix.

To calculate the transformation matrix A we just need to start from Equation 4.9 and isolate A, just as demonstrated in Equation 4.9.

$$T(x) = Ax \Rightarrow y = Ax \Leftrightarrow yx^{+} = Axx^{+} \Leftrightarrow yx^{+} = AI \Leftrightarrow yx^{+} = A \Leftrightarrow A = yx^{+} \tag{4.10}$$

According to Equation 4.10, A can be calculated by calculating the *dot* product between the samples coordinates (y) and the pseudo inverse of the body measurements (x).

After calculating A, we are able to map a vector of body measurements into a vector of coordinates with Equation 4.9. However, the result of that equation is a vector with $3v$ elements, 3 times more than the sample vertices, because while building the coordinates dataset we joined all vertices coordinates to form a 1-dimensional array. To represent a 3D shape from *T(x)* we just need to group the elements 3 by 3, resulting in a set of v 3D points.

5

Experimental Evaluation

The last Chapter described how we implemented both of our models and how we intended to compare them. In this Chapter we demonstrate how we compare the models and describe our validation and evaluation methodologies to reach the final answer to our question - what are the minimum body measurements required to recreate a realistic body shape?

We started by describing our methodology in Section 5.2, we divided our experimental evaluation process in two separate steps: validation and evaluation. The first step consists on testing both models using samples of the *Semantic Parametric Reshaping of Human Body Models* dataset [4] used to train both models and see which has better results. The best model was selected by comparing the body shape and measurements of the estimated shapes, with specific metrics explained in Section 5.2. The result of the validation process helped us to discard one model and use only one to perform evaluations with real users. After selecting the best model we proceeded to the second step - evaluation - and used the best model to estimate real body shapes of real users using only their body measurements. Finally, we presented our results in Section 5.3.

5.1 Methodology and Metrics

Our evaluation process was composed by two main processes: validation and evaluation itself. The validation process was defined within the set of processes and activities intended to verify that models are performing as expected, in line with their design objectives, and business uses. It also identifies potential limitations and assumptions, and assesses their possible impact. Thus, we validated our models with selected samples of the *Semantic Parametric Reshaping of Human Body Models* dataset [4] and observed if they performed well. More importantly, we observed which one performed the best and used the winner to the final evaluation process that involved real users. The validation and evaluation processes were qualitatively evaluated based on the estimations body shape and measurements. The estimated body measurements were expressed in centimeters and were directly compared to the original ones in both processes, we presented the estimated body measurements in Section 5.3.2.

The qualitatively evaluation of the body shape was more complicated. We validated both models by using four samples of the *Semantic Parametric Reshaping of Human Body Models* dataset [4], represented in Figure 5.1. This means that we had the meshes of the samples that we were estimating. By having both meshes available, we validated the performance of our models by directly comparing both shapes and see how much their shape differ from each other. Thus, we calculated the Mean Square Error, or simply *MSE*, that measures the average squared difference between the estimated values and the actual value. In statistics, the *MSE* of an estimator measures the average of the squares of the errors—that is, the average squared difference between the estimated values and the actual value. It is a measure of the quality of an estimator. As it is derived from the square of Euclidean distance, it is always a positive value with the error decreasing as the error approaches zero. In other words, as smaller the *MSE* value, the better is the estimator. We also measured the distance between correspondent vertices of the estimated and original meshes and presented a color map of the differences. This visual queue helped us to understand in which body zones our model had more difficulties to model and which ones are easier.

Relatively to the evaluation process, we validate the body shape of our estimated shapes by comparing the estimation, that resulted from the model with the best performance, with full body pictures of the individuals used for test. This process differs from the validation one by not having 3D meshes of the users that were used to evaluate our model. If we had 3D scans of those individuals, the evaluation methodology regarding the body shape would be similar to the validation one. Since we do not have 3D scans of the individuals, we took two full body pictures of their body: a frontal and a profile one. The individuals were asked to position themselves in a neutral pose similar to the pose that all meshes of the *Semantic Parametric Reshaping of Human Body Models* dataset [4] have - slightly open arms and legs - like represented in Figure 4.2. The pictures were taken at the hips level, to simulate the perspective of the estimations. Later, we extracted the body silhouettes of the pictures using *Photoshop*. We compared visually the pictures directly with the estimations, and we present the

results in Section 5.3. Finally, we selected which are the minimum essential body measurements to realistically estimate a body shape using only body measurements with the results obtained from the evaluation process.

5.2 Dataset

Both validation and evaluation processes are performed with the use of the *Semantic Parametric Reshaping of Human Body Models* dataset [4] to estimate new shapes. Essentially, the models were the same in both steps, only the test samples change: in the validation step we use the body measurements of four shapes of the *Semantic Parametric Reshaping of Human Body Models* dataset [4], while in evaluation step we will use body measurements of real individuals.

In the validation step we use four samples of the *Semantic Parametric Reshaping of Human Body Models* dataset [4], that are represented in Figure 5.1. These meshes were selected in order to represent the maximum variance in the human body. We have two males and two females, where in both gender we have a sample with a larger size and other one with a skinnier appearance. For the evaluation process, we used six different friends and family members. Unfortunately, we were not able to have a balanced testing sample regarding the gender. We tested five females and only one male. The age ranges of the tested people is in between 21 and 46 years, with the average being 23 years. We were not able to have a balanced test sample regarding the body shape, with most body shapes having a more slimmer appearance.

5.3 Results

We performed the experimental evaluation as explained in Section 5.2, we first validated our models to see if we had the desired outputs, and most importantly, to select the model that performed better. After selecting the best model to our problem, we evaluated it using real users. The validation procedure is described in detail in Section 5.3.1, while the evaluation one is detailed in Section 5.3.2.

Both validation and evaluation processes were evaluated in two main aspects: body shape and measurements of the returned estimations. The evaluation of the body measurements of the estimated mesh is a straightforward comparison between the body measurements of the original and estimated meshes - as smaller the measurements difference the better the model performed. This process applied both in validation as in evaluation steps. However the evaluation of the body shape is more complicated, and it is different for the validation and evaluation steps. In the validation step, since we used samples of the *Semantic Parametric Reshaping of Human Body Models* dataset [4], we had access to the original mesh, which means that we could

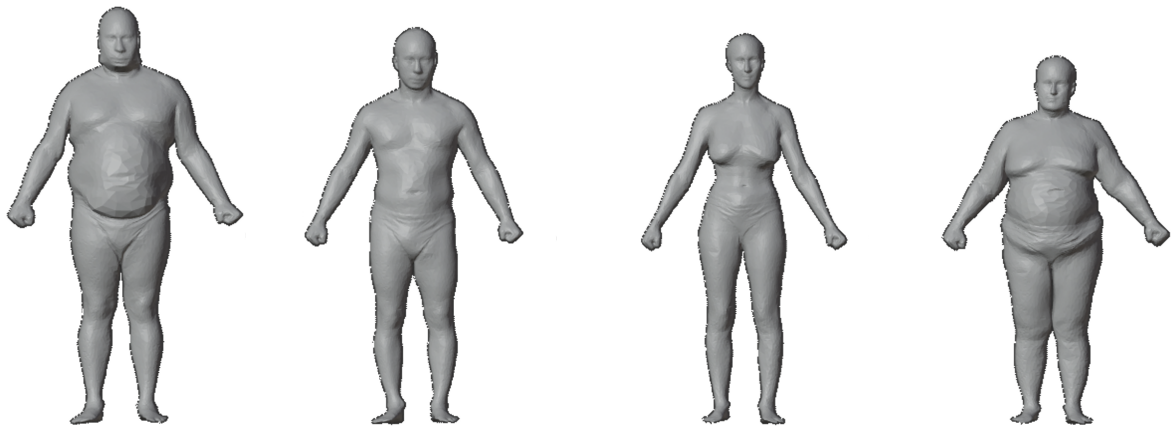

(a) SPRING0306. **(b)** SPRING0318. **(c)** SPRING0530. **(d)** SPRING0569.

Figure 5.1: Samples of the *Semantic Parametric Reshaping of Human Body Models* dataset [4] that will be used to validate our models. We choose samples that described the human shape variation the most, therefore the 2 shapes in the left are male and the 2 right ones are female. We also chose meshes that have a different body shape per gender, thus the meshes at the edges have a bigger size than the ones at the center.

directly compare the estimated mesh with the original one. We did it by calculating the *MSE* and the distance between correspondent vertices of the estimated and original shapes. This gave us a concrete way to measure how different both shapes were, as bigger the distance difference the correspondent vertices, less similar the meshes were in that particular body part. However, in evaluation step, we did not have access to the original 3D meshes of the individuals that tested our models. This forced us to evaluate our model performance, regarding the shape of the estimation, in a different way. We took full body pictures of the users and visually compared how similar the silhouettes were.

5.3.1 Validation

To first validate out approach before testing with real human users, we decided to test our model with four different samples from the database. These samples are represented in Figure 5.1. There were two male and two female scans with one having a smaller size and the other with a bigger size. The usage of samples that cover all spectrum of human shape was important to see if the models knew how to deal with all cases. First, we validated the accuracy of our model by evaluating the shape by comparing the estimated shape returns of our model with the original one. Finally, we validated the accuracy of our models regarding the body measurements by comparing the body measurements of the estimated shape with the original ones.

For both steps, we compared the results using several sets of body measurements, specially using the top ten and top seven measurements obtained from the feature selection process explained in Section 4.2.1. With

Mean Square Error														
Samples	***Top 2***		***Top 4***		***Top 6***		***Top 8***		***Top 10***		**Selected 6**		**Selected 7**	
	LIN	*PCA*	*LIN*	*PCA*	*LIN*	*PCA*	*LIN*	*PCA*	*LIN*	*PCA*	*LIN*	*PCA*	*LIN*	*PCA*
SPRING0306	0.0009	0.0574	0.0081	0.0296	0.0120	0.0150	0.0012	0.0020	0.0010	0.0008	0.0010	0.0026	0.0009	0.0028
SPRING0318	0.0032	0.0726	0.0024	0.0367	0.0017	0.0212	0.0013	0.0062	0.0009	0.0029	0.0022	0.0070	0.0020	0.0075
SPRING0530	0.0053	0.0945	0.0059	0.0396	0.0006	0.0062	0.0005	0.0045	0.0005	0.0003	0.0006	0.0059	0.0006	0.0062
SPRING0569	0.0017	0.0677	0.0018	0.0279	0.0017	0.0035	0.0026	0.0030	0.0017	0.0018	0.0017	0.0033	0.0019	0.0035

Table 5.1: Mean Square Error of the 40 estimations regarding the linear (LIN) and pca (PCA) models represented in Figures 5.2 and 5.4, respectively.

this, we can see if the process of feature selection correctly explains the variance of the human body and if the selected body measurements are enough to explain that variance.

Body Shape

The validation regarding the body shape was made by comparing the shape returned by the model with the original one by measuring the distance between the correspondent vertices. In other words, we compared the position of the vertices with the same index on the both shapes and calculate the Euclidean distance between them. This procedure was possible and not prone to errors due the point correspondence of the samples. With all distances calculated, we visualized the error using a color map, like represented in Figures 5.2 and 5.4. To validate both our models, we estimated the same shape using seven different body measurement subsets from the Table 4.6 and 4.7. Each column represents a different subset, and therefore a different estimation. From right to left in Figures 5.2 and 5.4: top 2, top 4, top 6 , top 8, top 10, selected 6, selected 7 and ground truth. By top X we mean how many measurements of the Table 4.6 we used. For instance, the first column used the top 2 measurements which corresponds to bust girth and hips girth (the first 2 measurements of the table) for both genders. The second column represents the estimations using the top 4 measurements corresponding to the top 2 measurements plus measurements 3 and 4 of Table 4.6 which are thigh girth and waist girth for males and abdomen and thigh for females. The same logic applies to all columns except the last one, that corresponds to the ground truth. In total, there are 28 different estimations distributed over 4 rows, resulting in 7 estimations per row. To address to a specific estimation we will use the nomenclature (xy) where x is the row number and y the column. Therefore estimation $(3c)$ corresponds to the one on the third row and column c, that represents the result of the estimation using the top 6 measurements of Table 4.6. The distance error color map is supported by the mean square error of all 56 estimations, represented in Table 5.1.

In both Figures 5.2 and 5.4, we understood that some body measurements configurations worked better than others. We saw that the results are often better when using more measurements. This is supported by Table 5.1 where the *MSE* values are higher as the number of measurements used to estimate a new shape increases. However, in Figure 5.2 we see that the difference between $(1d)$ and $(1e)$ is almost 0 and their MSE difference is

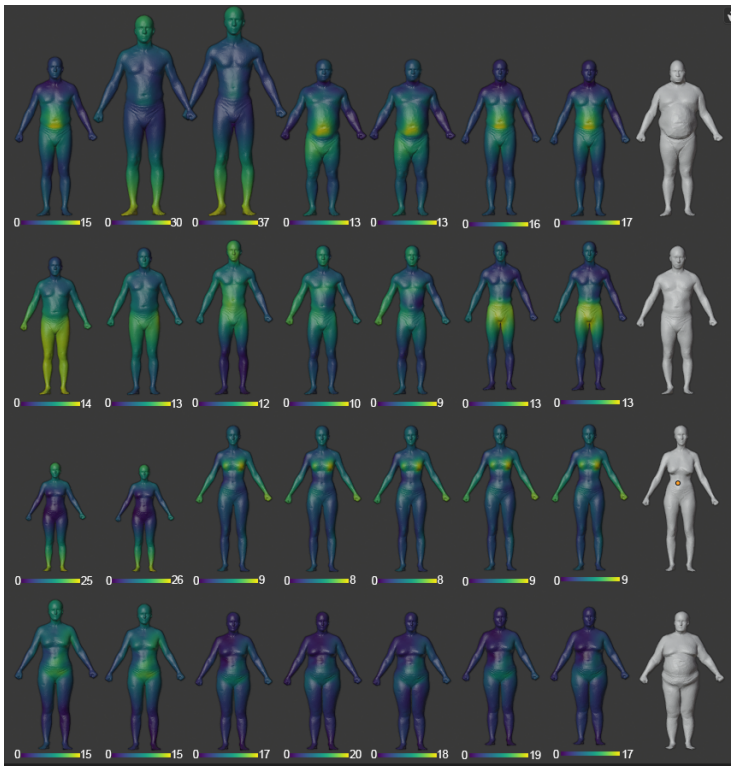

Figure 5.2: Error color map of the linear model using several body measurements sets. Each column corresponds to a subset of the top 10 body measurements represented in Table 4.6 or from the selected 7 from Table 4.7, from left to right: (a) top 2 (b) top 4 (c) top 6 (d) top 8 (e) top 10 (f) selected 6 (g) selected 7 (h) original shape. The yellow parts correspond to the parts that have a higher distance error in cm associated, while the dark blue parts are the ones that are more similar to the original shape.

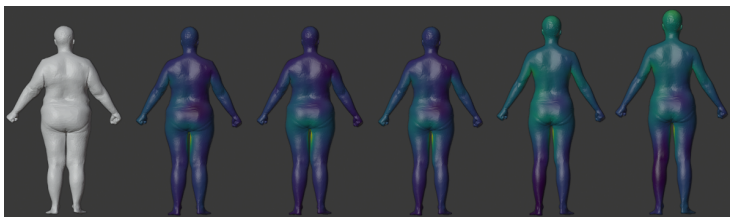

Figure 5.3: Back view of the fourth and final row of Figure 5.2.

Figure 5.4: Error color map of the pca model using several body measurements sets. Each column corresponds to a subset of the top 10 body measurements represented in Table 4.6 or from the selected 7 from Table 4.7, from left to right: (a) top 2 (b) top 4 (c) top 6 (d) top 8 (e) top 10 (f) selected 6 (g) selected 7 (h) original shape. The yellow parts correspond to the parts that have a higher distance error in cm associated, while the dark blue parts are the ones that are more similar to the original shape.

of about 0.0002. This indicates that the insertion of the body measurements 9 and 10 of Table 4.6 is irrelevant, and we obtained the same results using only the first eigth measurements. In (*1c*) of Figure 5.2 we notice a big difference in the height comparing the original sample. This happens specially to male meshes because the height is not part of the top six measurements according to Table 4.6, however it is more noticeable in (*1c*) than in (*2c*). This happens because of the high values of the remaining measurements, like waist bust, abdomen, etc. Sample *SPRING306*'s body measurements are way higher than average on the dataset and there are not many samples with bigger sizes, the model estimates a new shape using the information that it has. This results in a shape that is very similar to the average male body, but in a bigger scale. This explains why in (*1b*) and (*1c*) of Figure 4.6 have a higher distance difference of sample *SPRING0306* in their feet and head, since the center of all meshes is on their groin. To produce a shape with such big measurements, the model scales the shape in order to respect them and the model ends up being huge because in top 6 measurements we do not have height as a constraint. This effect is also visible in (*1b*) regarding the top 4 measurements, however in (*1a*) it is not visible. It is visible that in (*1a*), (*1b*) and (*1c*) the main differences regarding the original mesh are in the belly. Sample *SPRING0306* (*1g*) is characterized by having larger dimensions and our linear model may have difficulties representing those dimensions to perfection. However it is able to return a shape with larger dimensions but not as big as the ones inserted. This may be happening because groups of male with larger dimensions are poorly represented in the *Semantic Parametric Reshaping of Human Body Models* dataset [4]. The estimation represented in (*1a*) is very similar to the ones of columns (*1d*) and (*1e*), it even has a similar maximum error (15cm) but it fails to represent the belly in a more similar way. We expected the columns (*1g*) and (*1g*) to perform better since the subsets are composed by body measurements that were obtained through feature selection, represented in Table 4.7. But the absence of the measurements like rise length and/or under-bust to belly button had a negative impact on the returned shape, especially on the belly of the estimations were they have a higher distance error. By analyzing the results of the estimation of sample *SPRING0306* and its MSE values, we conclude that the best subset of body measurements is the top 8.

Regarding the estimation of sample *SPRING0318* using the linear model, all subsets returned a mesh that is similar to the original one, even columns (*b*) and (*c*) of Figure 5.2, that on the first row were scaled to non human dimensions, returned good results. This is because the body measurements of sample *SPRING0318* (*2g*) are similar to the average ones of the dataset, which means that this sample belongs to a group that is well represented in the dataset. Analyzing this second row from right to left, (*2e*) is very similar in shape to (*2h*) with a bigger difference on the bust and groin areas that are hardly perceptible to the human eye. There is a difference of 0.0004 in their MSE values which is very close to 0. It has a maximum difference of 9cm on the left hand, because the dataset was not normalized in terms of pose, therefore estimations have slightly different poses which affects this color map. (*2d*) is also very similar to the original sample (*2g*), with results almost identical to (*2e*). Once again, the top 8 subset has very similar results to the top 10 subset. (*2c*) is the one that differs the most,

it returns a taller and skinnier shape that differs from (*2g*) in the torso and groin area, reaching 12cm distance of difference. Both (*2a*) and (*2b*) differ the most from the original mesh on the legs, however, (*2b*) has less error than (*2a*). (*2a*) has a big distance difference from the original sample in the legs, mainly because of pose, the original sample has more curved legs than the original one, which affects the results. The subset that returned the best results was (*2e*) representing the top 10 subset, however, since the top 8 has almost no difference from it and uses less 2 measurements, this subset is preferred over the top 10 one. Top 8 wins over top 2 because top 2 returns a mesh that is smaller than the original one, this happens for the same reason that (*2b*) and (*2c*) return a shape with a a bigger height, it scales the estimated shape into fitting the inserted measurements, and since the height is not a constraint, it only considers the top 2 measurements. Once again, estimations (*2g*) and (*2g*) produced shapes that are not very similar to the ground truth (*2h*). The lack of the rise length and underbust to belly button length proved to be necessary for males once more, with the biggest distance error being on the groin, an area that is covered by the rise length. Therefore, considering these 2 male samples and the subsets used to validate our linear model, we conclude that the top 8 and top 10 subsets return more accurate results that are very similar, but since top 8 uses less 2 measurements, it is preferred since it returns results almost identical to the top 10 subset.

We analyzed the results regarding the male body estimation, now for analyzing the performance of the model for female shape, we did the same procedure that we did with the male shapes for the female shapes - *SPRING0530* (*3g*) and *SPRING0569* (*4g*). First, shape *SPRING0530* is characterized by having a more slim figure while *SPRING0569* has larger dimensions. Lets first analyze the results of estimating *SPRING0530* with our linear model, the results are represented in the third row of Figure 5.2. Overall, all subsets with exception of (*3a*) and (*3b*) returned a shape that is very similar to the original one (*3g*), with the maximum distance error being 9cm on the breast and MSE values that differ by 0.0001. The effects of the slight pose differences are visible especially on the right hand of the estimations. The top 6 subset estimates a shape (*3c*) that is very similar to the original one, which does not happen in male estimation, because the top 6 female subset is different from the male one. The female one contains the height as a constraint, while the male one does not. This permits the linear model to output a shape that is more realistic and much more similar to the original one. Comparing all 3 estimations from these subsets, the (*3c*) one is better because it uses less measurements for almost the same result. (*3b*) and (*3a*) are shapes with smaller stature, and since it does not contain height as a constraint, it scaled the result to fit the inserted measurements. These results can be compared with (*1b*) and (*1c*), where the results were also scaled into abnormal statures, with the main distance error being on the feet and head.

The result of the estimations in the forth and final row of Figure 5.2 is very similar to the ones of the third row. Columns (*c*), (*d*), (*e*), (*g*) and (g) provide estimations that are very similar among them, however they are all slightly different from the original one (*4g*). Sample *SPRING0569* has a very square figure, while the estimations

provide an hourglass shape. The main distance error is on the interior of the thighs that can be seen in Figure 5.3, that represents the back view of the final row of Figure 5.2. Even with a more similar shape, these subsets have a higher distance error than the subsets top 4 and top 2. Columns (*a*) and (*b*) scale the output to fit the inserted measurements and return a shape with a bigger height than supposed. Top 8 subset was the one that best performed estimating shape *SPRING0569* by providing results almost identical to the top 10 subset. However, the shape is slightly different from the original one, just like in the first row. Just like sample *SPRING0306*, sample *SPRING0569* is characterized by having a larger size, and therefore higher body measurement values. Both samples belong to a group that is poorly represented in the dataset, thus the linear model has more difficulty estimating them.

Overall, the top 8 subset was the one that best performed, with exception of the top 6 subset on the third row of Figure 5.2. This subset always returned results that were almost identical to the ones returned by the top 10 subset, which makes them preferable because they provide the same results using less information. Only the female samples were correctly estimated regarding the subsets of Table 4.7. One possible reason for this to happen is that the selected 6 subset obtained from Table 4.7 is identical to the top 6 one from Table 4.6. With this we conclude that the rise length and the underbust to belly button measurements improve the shape accuracy of the linear model. Regarding the second model, produced by performing the PCA on the dataset and relating it to the body measurements, the result of estimating the samples of Figure 5.1 using the same subsets is represented in Figure 5.4. Just like in Figure 5.2, this image has 4 rows, each one containing estimations for a different sample and 6 rows: top 10, top 8, top 6, top 4, top 2 and ground truth from left to right. The column (*a*) regarding the top 10 subset uses all 10 measurements from Table 4.6, column (*b*) only uses the first 8 measurements from the table, and the rule applies to all the first 5 columns. These 5 columns were compared, in terms of their shape, with the original shape represented in column (*g*).

Overall, the pca model performed worst than the linear model, with the principal feature of returning shapes with abnormal heights which made its MSE value increase. The returned model is taller as fewer measurements are inserted, and therefore the distance error increases with the maximum on the head or/and the feet. Only the column (*e*) returned shapes that were slightly similar to the original one, in other words the height is similar however the shape is not. Comparing the results of the male shapes, both results of the top 10 subset returned a shape that is similar, even with the original body measurements being completely different. The fact that sample *SPRING0306* had bigger measurements had no impact on the estimation, the torso is not larger than the estimation of the second row. And it translates to the distance error being more prevalent in the belly area, reaching 15cm near the belly button, while in the second row the error is more sparse. The same happens with the female estimations (*3e*) and (*4e*), they are almost identical and the fact that (*4h*) has larger dimensions has no impact on (*4e*). The estimations (*2e*) and (*3e*) are very similar to their original shapes (*2g*) and (*3g*), the fact

that the error reaches a value of 13cm in (*3e*) and 5cm in (*3e*) may be because of pose differences. However (*3e*) is slightly different from (*3e*), the differences are visible in the waist were it is marked with a more green color. The fact that (*3e*) contains less distance error than (*2e*), even if (*2e*) is more similar to (*2g*) than (*3e*) is to (3f), is because (*3e*) has a more similar pose to (*3g*) than (*2e*) to (*2g*).

Comparing the results of our linear model, represented in Figure 5.2, and our pca model, represented in Figure 5.4, with the support of their MSE values represented in Table 5.1, the linear model is more able to adapt to new shapes that are not well represented in the dataset. The PCA model did not adapt to shapes that were not the standard, while the linear model did. This versatility made the linear model to be preferred over the PCA one. As seen in Figure 5.2, the Principal Component Analysis did not have a trustful outcome, something that Yipin Yang also concluded in [4] with his global mapping methodology. He concluded that the model has difficulty with overfitting especially when a smaller dataset is used. Since *PCA* coefficients do not have actual meaning as to anthropometry, we must treat all semantic parameters equally for each *PCA* coefficient. Consequently, the topology of human body is ignored. One reason might be the impossibility of classifying a principal component relatively to a measurement. By other words, it is impossible to know what measurements directly affect the principal components of the *PCA* analysis. In Figure 5.5 are represented the 4 principal components of the male (5.5(b)) and female (5.5(a)) datasets. These components are the ones that will affect the final result of the *PCA* model, however only components 1 and 3 have more visible changes, while the components 2 and 4 have less visible changes. One thing that we also noticed is that the components do not only have a shape variation, they also have a pose variation. This is bad because it makes the *PCA* to capture the pose as a variation instead of the shape itself and it shows up in the results.

Since we are mapping these components directly to a set of body shape measurements, as smaller the set, the more information regarding the body shape variation each measurement will have. And since it is impossible to directly connect a measurement to a specific change in the human body represented by a PCA principal component, any measurement could have information of the bust, hips or even height. This might help explain why the results presented in Figure 5.4, where as smaller the measurement set is the taller the estimation is. The usage of the *PCA* to map a new body shape turned impracticable to create new body shapes, especially because all shapes returned were very similar, even when the original measurements and the measurement subset used to train the model differ. In Figure 5.4 we see that results from line 1 to 2 are practically identical, and the same happens to line 3 and 4. The incapability of this model to adapt to different body shapes is one of the reasons why this model is not reliable for a virtual fitting room, the other reason is the incapability to directly map a measure to a specific part of the body variation (principal component).

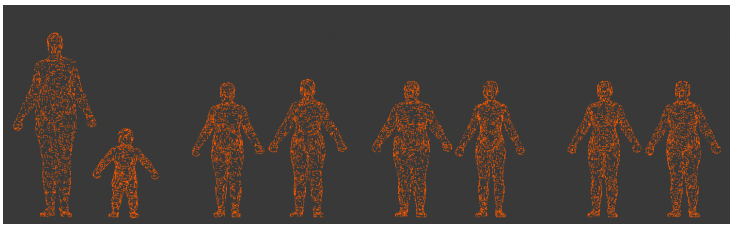

(a) Female 4 principal components.

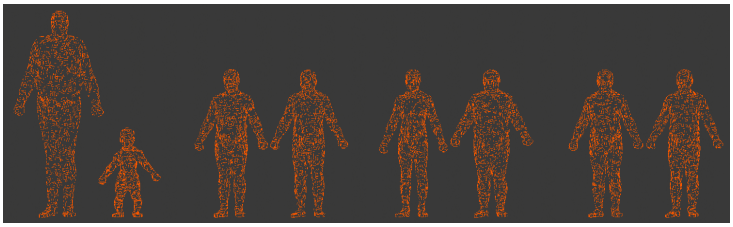

(b) Male 4 principal components.

Figure 5.5: The principal components resulting from the *PCA* on male and female datasets. Each cloud point corresponds to the visualization of the template mesh with the sum of an eigenvector scaled by its eigenvalue with a multiplication factor (-2 and 2).

Body Measurements

The validation regarding the body measurements was made by comparing the body measurements extracted from the estimated shapes with the original ones. The body measurement extraction of the estimated shapes was made just like the extraction of the measurements of the original shape was made. The body measurements are represented in Tables B.1, B.2, B.3 and B.4 and in their correspondent Figures 5.6(a), 5.6(b), 5.6(c) and 5.6(d). Just like in the previous section, we have the results of 7 different estimations using 7 different subsets obtained from Tables 4.6 and 4.7. The body measurements represented here were extracted from the estimations displayed in Figures 5.2 and 5.4. In all 4 tables, the first column is reserved for the true value of the sample's measurements, which is accompanied by a black bar on Figures 5.6(a), 5.6(b), 5.6(c) and 5.6(d). The remaining columns represent the same measurements extracted from the estimations that are accompanied by colored bars on the same Figures.

We demonstrated on Section 5.3.1, that our models cannot estimate shapes that are less represented in the dataset, especially samples with large dimensions. In this section, we will analyze those shape measurements. At first sight of Figures 5.6(b) and 5.6(c), the linear model was able to estimate both samples *SPRING0530* and *SPRING0318* only with a few exceptions on the top 4 and top 2 subsets, with the height difference of 47cm on Table B.1. However, we have already excluded this two subsets by analyzing Figures 5.2. On the other hand, the PCA model proved to fail in estimating a human shape that has a similar body shape to the original mesh. Any

estimation derived from the PCA model was able to fit the desired measurement set, thus we conclude that this model is unusable.

Overall, our linear model was able to estimate *SPRING0530* and *SPRING0318* better than *SPRING0569* and *SPRING0306*, because the first ones belong to a group that is well represented in the dataset. This makes the measurements of the estimations of samples *SPRING0530* and *SPRING0318* to be more similar to the original ones. In Table B.3, that correspond to the body measurements of *SPRING0530*, we see that all subsets, except for top 4 and top 2, performed relatively well with a bigger error rate on the girth measurements. Thus, since the usage of the subsets obtained from Table 4.7 do not produce better results, we will discard them for the rest of this document, only focusing on the subsets obtained from the Table 4.6.

5.3.2 Evaluation

The evaluation with real users was practically the same as validating synthetic meshes in Section 5.3.2. We inserted the measurements of the meshes that we want to estimate in our model and compare the returned shape with the original one. However, testing with real users means that it does not exist an original mesh to compare the estimated one. To compare the returned mesh with the shape of the individual, we take a picture and extract the silhouette and compare it with the estimation. Finally, the evaluation of the body measurements is the same as the one described in Section 5.3.1. We extract the body measurements of the estimated mesh and compare them to the original ones. In Section 5.3.2 we explain how the visual validation was performed and discuss the results, while on Section 5.3.2 we analyze the results of the body measurements of the estimated meshes.

Body Shape

To evaluate our model regarding the estimation of real users body shape, we took two pictures of the users: a frontal and a profile one. Since we deal with sensible information on this thesis, we wanted to protect our testers identification. We did this by only using the silhouettes of their body shape, instead of the raw pictures.

First of all, we took pictures of the testers body. Then, we contoured the silhouettes by using *Adobe Photoshop* and removed the filling of the images, resulting only the silhouettes of the users. These images were placed side by side on their body estimation meshes, in Figure 5.7 we can see the final results. In the image, most of the silhouettes head shape looks strange because of the users hair. The hair makes it difficult to trace a perfect contour of the user, however, since the head shape is not the goal of our model, it should be ignored in the analysis as a result. By observing Figure 5.7 we can see that the model succeeded in presenting an estimation that is very similar to the original body shape of the users. However the results are not perfect, overall our model

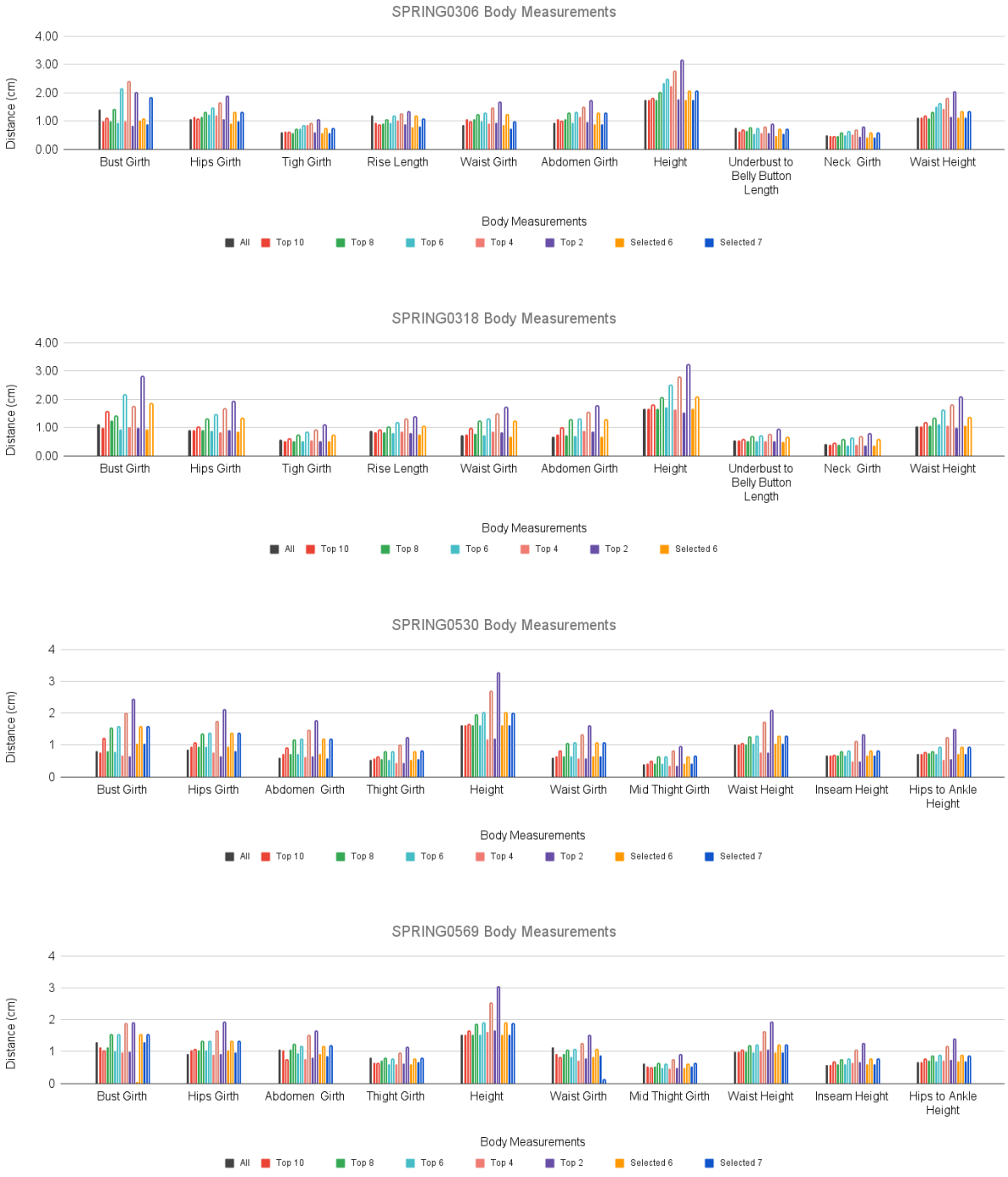

Figure 5.6: Body measurement values regarding the estimations with 7 different subsets using the linear (*LIN*) and PCA (*PCA*) models. The solid bars (with the exception of the first black one) correspond to the measurements extracted from the estimations derived from the linear model (*LIN*), while the hollow bars with a colored stroke correspond to measurements extracted from the estimations derived from the PCA model (*PCA*). Each subset used is represented with a distinct color, and the differentiation between the models is the bars filling.

seems to have difficulty representing zones that have more body fat, especially on the thigh and abdomen. This problem could probably been solved by adding the body fat percentage of the samples on the dataset, however we need to know that information about the users as well. It is important do underline the fact that we are only evaluating the body shape of the estimations, excluding head, hands and feet. Therefore we are only focusing on the torso, arms and legs of the estimation. The head of the silhouettes has random forms because of the hair of the users. While extracting the silhouettes, the hair is a complicated area, specially in a background that is not of a single solid color. Therefore, only the torso, legs and arms are to be considered in Figure 5.7.

The perspective of the silhouettes and the estimations is not the same, and impacts the comparison between the estimations and the original silhouettes in Figure 5.7. Each user was asked to take their own pictures at the hip level to be as similar as possible to the perspective of the meshes in *Blender* software. However it is impossible to recreate that perspective in the real words, which makes the silhouettes to contain visible artifacts that the estimations do not have, like the instep, or the 2 feet in the profile silhouette - the left foot is visible on the calf level. The different perspective between silhouettes and estimations also gives the impression that the estimations have bigger height measurements than the silhouettes. While creating Figure 5.7, we tried to align the shoulders and the ankles of the silhouettes to the shoulders and ankles of the estimation. As we demonstrate in Section 5.3.2 the height measurements are the ones that performed the better in general, with estimations very similar to the original ones. Thus, the height difference given by the different perspective among the estimations and respective silhouettes, is nothing else but a perspective trick.

We noticed that our model has difficulty on model the waist of estimations. In cases where the original shape has hips relatively larger than the waist, as *P3* does, our model returns a shape with a larger waist than it should. However our model estimates shapes with a waist relatively similar to the hips as having smaller waists. Almost every users are considered to be part of the group that is well represented in the dataset: A more slim appearance for both represented genders, and for females a waist that is thinner that the hip. This made possible for our model to return better estimations regarding *P1*, *P2*, *P3*, *P4* and *P5*. Since *P6* belongs to a group that is poorly represented in the dataset, the model struggled to estimate its shape based only in measurements. The inclusion of body types as inputs could improve the estimations. When inserting information about its body, if a user were asked to insert the shape of their belly and/or hip, etc, the model would not only the measurements, but also the shape of the user's body to rely on. Also, if we implemented a model for each body part, instead of a single one that estimates a new shape as a whole, and used the body measurements and a specific body part shape we would have more information about how a specific body part should be. If a user inserted *70cm* as waist girth and an hourglass as body shape, the model would know that the estimation must have a waist that is thinner than the hip. By other hand, if a user inserted a square as a body shape, the model would know that the estimation must have a hip girth similar to the waist. A possible consequence of modeling each body part

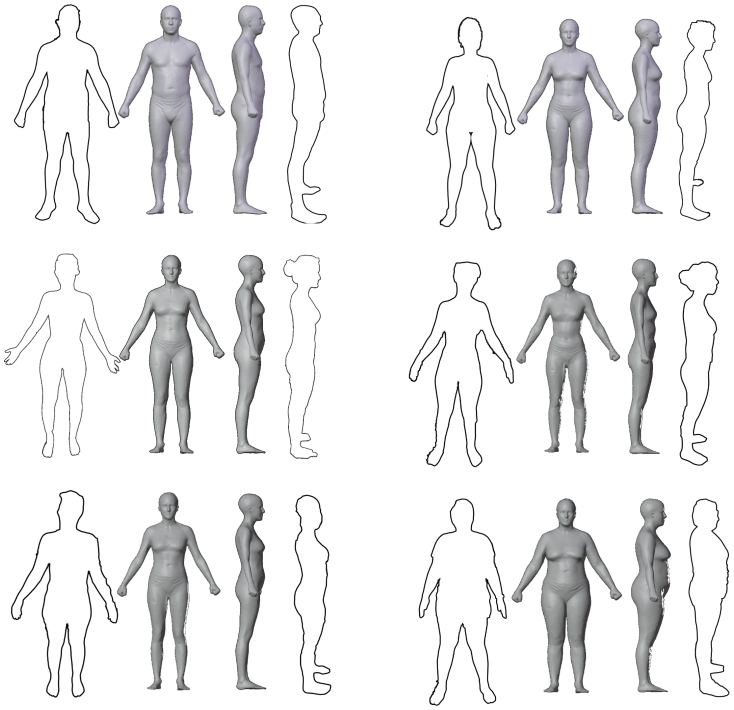

Figure 5.7: Visual comparison of real users silhouette with their correspondent shape estimation using the top 8 measurements subset. From left to right and top to bottom we called these estimations *P1*, *P2*, *P3*, *P4*, *P5* and *P6*.

separately is in the joints of those said body parts. Different models return different estimations that are independent from each other, which means that the estimated arm may not be perfectly lined up with the estimated torso.

Besides the waist, our model also had difficulties on estimating fuller thighs. *P2* is a good example, we see that the frontal silhouette (the first image counting from the right of *P2*) has fuller thighs, something that the estimation does not. It has an indication of fuller external thighs, however the interior of the thighs is not very similar. The estimations presented in Figure 5.7 are not perfect representations of the users silhouettes, the model had difficulties on correctly estimate waits and thighs. However the estimation returned new shapes that are pretty similar to the original ones. We asked the users if the estimation was similar to their bodies, they pointed some issues like the waist and thighs but said that overall it looked like them. We conclude that our model is capable of estimate a new body shape according to a small set of body measurements input.

Body Measurements

We also evaluated the body measurements of the estimations and compared them with the original ones. The results of the body measurements together with the results of body shape detailed in Section 5.3.2, will help us decide which measurements are required to estimate a new body shape. The results obtained from

	Real Users Body Measurements											
	P1		***P2***		***P3***		***P4***		***P5***		***P6***	
	T	*E*	*T*	*E*	*T*	*E*	*T*	*E*	*T*	*E*	*T*	*E*
Bust Girth	0.98	1.00	0.80	0.81	0.90	0.89	1.04	1.00	0.87	0.85	0.83	0.78
Hips Girth	0.99	1.06	1.03	0.99	1.05	1.00	1.13	1.01	1.03	0.92	0.95	0.92
Thight Girth	0.57	0.59	0.59	0.62	0.56	0.63	0.63	0.69	0.58	0.52	0.55	0.53
Waist Girth	0.89	0.91	0.67	0.63	0.68	0.69	0.95	0.70	0.74	0.72	0.6	0.62
Abdomen Girth	0.99	0.93	0.83	0.62	0.84	0.63	1.04	0.73	0.84	0.73	0.74	0.73
Height	1.78	1.80	1.62	1.62	1.74	1.74	1.57	1.57	1.60	1.60	1.57	1.57
Underbust to Belly Button Length	0.20	0.18	-	-	-	-	-	-	-	-	-	-
Neck Girth	0.39	0.43	-	-	-	-	-	-	-	-	-	-
Rise Length	0.98	0.95	-	-	-	-	-	-	-	-	-	-
Waist Height	1.14	1.20	1.02	1.02	1.13	1.13	1.02	1.02	1.05	1.05	0.96	0.96
Inseam Height	-	-	0.73	0.66	0.85	0.72	0.72	0.63	0.74	0.67	0.71	0.64
Mid Thight Girth	-	-	0.5	0.46	0.43	0.43	0.57	0.52	0.3	0.38	0.35	0.4
Hips to Ankle Height	-	-	0.95	0.73	0.92	0.79	0.7	0.72	0.77	0.73	0.67	0.69

Table 5.2: Body measurements extracted from the estimations of the six people represented in Figure 5.7. We show the original measurement value (*T*) and the estimated one (*E*) of each user side by side. Numeration between this table and Figure 5.7 are in correspondence, which means that the *P1* in this table corresponds to the *P1* of Figure 5.7. The new shapes were estimated using the top 8 measurement subset of Table 4.6. *P1* corresponds to a male person while the others are female. We validated the male and female meshes according to its correspondent top 10 measurements according to Table 4.6, this way the male mesh was only evaluated concerning the top 10 measurements that vary the most on male bodies while females were evaluated with their corresponding top 10 measurements that vary the most.

measuring estimations are represented in a table form in Table 5.2 and in a visual form in Figure 5.8. The results presented here correspond to the estimations of six different people, represented as *P1*, *P2*, *P3*, *P4*, *P5* and *P6*. These representations are in correspondence to the results presented in Figure 5.7, which means that the measurements of *P1* in Table 5.2 correspond to shape *P1* of Figure 5.7. This makes it easier to compare the results and to relate body measurements to body shape.

The first thing that we noticed is that, the estimated height and waist height measurements in female estimations were the same as the original ones. This means that these measurements did not have any kind of error, and that the visible difference in height in Figure 5.7 was caused by the perspective and nothing else. However, the inseam height and hips to ankle height measurements had some errors associated. In inseam height, the estimation was off by 12cm in some cases. We realized that this is because people found it difficult to understand how they should measure the inseam height, therefore all users measured it differently. In Table 4.1, we explain that the inseam height is the distance between the lower groin point and the ankle, but people found it difficult to understand which is the lower point of the groin. Given this, everyone assumed that the lower groin point was in a different spot, what had a negative impact on the estimations, and consequently, on the measurements. On other hand, our only male sample showed some errors associated with the height

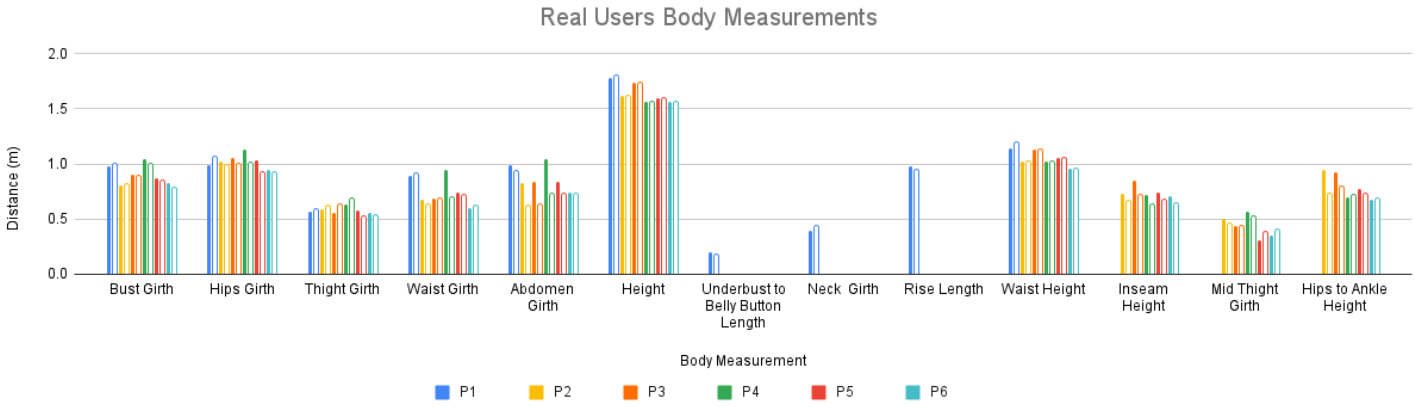

Figure 5.8: Visual representation of Table 5.2. Each user tested corresponds to a different color, where the solid bar corresponds to the real measurement value (ground truth of a specific person) and the hollow one the measurement estimated value. We show the original measurement value and the estimated one of each user side by side to simplify the comparison.

measurements, especially in the waist height one. We do not have test samples to support this, but we believe that is because of the fluctuation of the waist point in the dataset meshes. All measurements were extracted from defined vertices that were manually selected. This means that all waist girth measurements of all meshes used the same 2 vertices, but those vertices, specially the one on the waist, fluctuates. Even that it means that this vertex will always be part of the belly, depending on the dimensions of the mesh, the vertex might be positioned bellow or above the waist line, which can lead to errors.

The measurement that had more error associated was abdomen girth, with a distance difference reaching up to *31cm*. We believe that this is also because the vertex fluctuations on the meshes, and the girth extracted might sometimes be more similar to the waist than the abdomen itself. If we keep feeding our module with samples that have smaller shapes but we say that have higher measurements values, our model will assume that higher measurements values means a smaller shape. Something similar happens in almost every girth measurements, in a smaller scale. The estimations of the bust girth are usually smaller than the original one, reaching a distance difference of *5cm* in the worst case. We observed that some measurements not behave like this: thigh girth and mid-thigh girth estimations had a higher measurement value than the original one.

Total distance error (*TDE*) is the sum of all distance errors between the original (T) and estimated (E) measurements. This value helps us understand which body shapes our model struggles more (or less) to estimate according to a measurement constraint. The *TDE* per user is $TDE_{P1} = 36cm$, $TDE_{P2} = 66cm$, $TDE_{P3} = 61cm$, $TDE_{P4} = 84cm$, $TDE_{P5} = 51cm$ and $TDE_{P6} = 27cm$. *P6* is the shape with less *TDE* given it is the shape that differs the most from the original one according to Figure 5.7, with an estimated waist far thinner than the original one. On average, female estimations had a *TDE* of *57.5cm, 21.8cm* higher than the male one. According

to the results, our model estimated more accurately the new shape measurements that have higher dimensions, but in this case the body shape is far different from the original one. The opposite also applied, more thinner shapes originated estimations that have a similar body shape but with a high *TDE* value, normally estimating measurements that are way smaller.

The analyze of the body measurements of Table 5.2 made us believe that this model is not suitable for a virtual dressing room, because it estimates new body shapes with some significant *TDE* values. We believe that most of this error is because of vertex fluctuations that impact body measurements in the preprocessing step.

We conclude that the final measurement subset should be the top 8 for the male estimations, to maximize the amount of information about the belly as possible. The final measurement subset for female estimations is the selected 7 that includes the mid-thigh girth that is fundamental in the female body estimation.

6

Conclusion

The main goal of this thesis is to discover the minimum subset of body measurements that describe the maximum of human body variation. To discover that final subset we extracted the body measurements of the *Semantic Parametric Reshaping of Human Body Models* dataset [4] and trained two different models with it. Our approach involved the comparison of the two models, one using pca weights and the other using linear transformations to estimate new shapes. The comparison of both models was also useful to see if the usage of PCA weights has any positive influence on the estimation of new shapes compared to a straightforward approach of mapping the vertex coordinates directly to the body measurements.

We validated both models using samples of the dataset regarding their estimated body shape and body measurements and selected the one with better results to the final evaluation step using real users. From observing the estimations provided by the best model - the linear model. We then selected the subset that estimated new shapes that were more similar to the original ones. This subset corresponded to the top 8 measurements represented in Table 4.6, by other words, the best subset was the one that used the first 8 measurements from the top 10 subset represented in Table 4.6.

Once completed the validation process, we evaluated our model using the linear model using the top 8 measurements subset. Just like in the validation step, we evaluated the estimations regarding the estimated body shape and measurements and reached the conclusion that our model is not appropriate to estimate new shapes with similar body measurements as the original shape. And since this thesis is targeted for a virtual dressing room, it brings concerns on how similar the estimation is to the real user if both the estimation and user do not have the same measurements. Instead of helping the user on choosing a size, it may mislead the user into buying the wrong size. On the other side, our model was able to provide new body shapes that were very similar to the original ones. This was also supported by the users, because the majority said that the estimation had a similar shape as them.

6.1 Limitations

This section is destined to list this thesis limitations. This was a very interesting thesis to work on, however there are several things that can be improved. These limitations are related to the main complications of the application, which means that all can be improved.

The first limitation is presented before the thesis started, the dataset used was the *Semantic Parametric Reshaping of Human Body Models* [4], however this was not the best dataset for this thesis. As explained in Section 4.1.1 the best dataset would be the *CAESAR* dataset, however it is not available for research purposes. *CAESAR* dataset was appropriated for this thesis because beside it contains a large 3D scan collection of real people, it has landmarks as well, by other words, body measurements. Since the used dataset did not contain any body landmarks, like *CAESER*, we had to extract them ourselves.

In Section 4.1.4 we describe the process of extracting the body measurements. We use 3 different measurements: length, height and girth explained in Sections 4.1.4, 4.1.4 and 4.1.4, respectively. The first two measurements are not perfect, however the results did not gave any extra problem, which means that they could be immediately used without any kind of extra processing. The girth measure was the most complicated one because of the pose of the meshes. It is important to notice that we do not normalize our meshes pose, which can lead to measurements errors. By not normalizing the pose of our meshes, it means that all of them are on a slightly different pose, this happens because the dataset is based on 3D scans of real people. It is impossible for humans to be stand still, there are always small movements that are invisible to the human eye, and it is also almost impossible to replicate the exactly the same pose among several people. These human flaws bring pose differences that can affect measurements on the meshes when we are extracting the body measurements.

Besides the slightly pose differences, there is also the issue of we extract the body measurements directly of the meshes on how they are on the dataset. These meshes are in a neutral pose with the arms and legs a bit opened, like it is represented in Figure 4.2. This specific pose is complicated to extract measurements on the bust zone, specially if the mesh has larger dimensions. If we extracted the bust on those meshes, the value would include the arms as well, because of the meshes intersection. To resolve this problem we developed a classification model to classify new points, derived from the intersection between the mesh to be measured and the horizontal plane, in the correct body according the K-nearest neighbors, this process is explained in detail in Section 4.1.4. Basically, we exclude the new vertices, derived from the intersection, that are not classified within the body part that we are measuring. For instance, to measure the bust girth we exclude the new vertices that were classified as belonging to the arms. This solution works, however it is not ideal because we do not reconstruct the excluded vertices. This leaves 2 holes, in the intersection line, that correspond to both arms. Since the value of the bust girth (and any other girth measurement) is the sum of the length of all edges, the holes decrease that value. We solve that by assuming that the missing distance is the euclidean distance between the tail vertices, however that value might be wrong because it does not consider the curvature of the body. This problem could be solved by positioning all meshes in T-pose before extracting the body measurements, however that process is complex.

The imperfection of the measurement extraction method could be easily repaired if we had access to the body landmarks of the people that were scanned to produce the database. The fact that the measurements that we extracted from the meshes of the dataset are not perfect, impacts both of our models. In the model generation phase, we believe that those imperfections impact the performance of our model, especially the girth measurements. In Section 5, we presented the body measurements differences between the original and the estimated models and the measurements that contain more errors are the girth ones. By other hand, the height measurements are almost perfect. We believe that if the girth measurements were correct, the differences between the original and estimation models would be far less. Our models are also not able to replicate the shape in a perfect way, especially with larger dimensions. A good example of this is represented in Figure 5.2, in the final row we estimate a female mesh with larger dimensions, however the estimated shape is not similar with the original one. The original shape has the waist and hips at the same level, while the estimated mesh has a thinner waist. We believe that this issue could be improved by inserting a 2 pictures of the user: a frontal and a profile one, in order to extract the shape. With the silhouette of the images and the measurements the results would, possibly, improve a lot.

The comparison between both models showed that the usage of PCA is not beneficial for the body shape estimation, in Figure 5.4 we see that the estimation results in abnormalities. The linear model presented in much better results, with body shape and measurements quite similar to the original ones. However it showed

difficulty on estimating shapes that were poorly represented in the dataset. Shapes with bigger dimensions were the ones that performed the worse, with estimations that were smaller than the original ones. This is a problem because it does not correctly represent the individual that is being estimated, and since this thesis has a virtual fitting room in mind, this means that a person could be mislead into buying the wrong size. The usage of body pictures would prevent this by shaping the original body more accurately with the desired body measurements.

6.2 Future Work

In the previous section we talked about the limitations of this thesis, and therefore the first step to improve the performance of this thesis is to improve the parts of the system that are diminishing the quality of the results. Including pose normalization to put the meshes in a better position while extracting the measurements, or get a dataset that already contains those body landmarks, as well the position of the joints. The pose normalization would allow the manipulation of the meshes in a way that it was possible to put them in a T-pose to better extract measurements surrounding the bust. Training our linear model with more samples would also be beneficial to incorporate more body shapes. The inclusion of more body shapes would decrease the possibility of estimating a new shape that was not partially learned already, increasing the accuracy of the model.

However, this thesis was made with the goal of creating a realistic virtual fitting room, and a realistic virtual fitting room requires a realistic avatar. This avatar would, ideally, look like the person that it is trying to simulate, and for that it needs a realistic face and textures and not just a realistic 3D body shape with a solid grey texture. Therefore, a realistic face needs to be calculated for this model, and the best solution was to use a camera. Photogrammetry scanning is the process of creating a 3D object entirely from images. It could be a great start, however it requires some preprocessing treatment. The usage of *Light Detection and Ranging* (*LIDAR*) technologies, could also be a good idea, since the *Lidar* scan measures the distance of a point in the environment in a similar way as the sonars do, but instead of using the sound, they use the light itself. The good about these cameras is that they not only capture the light in the environment, they can also tell how far away are the objects in the environment from the scan, making these cameras great for *Augmented Reality* purposes.

The inclusion of a realistic face based on a photo, and skin like texture, all together with a realistic body shape would complete the realistic avatar based on a real person. With the inclusion of animations, especially facial animations would bring the avatar to life, making it possible to export it and use it in games, or even conferences in some virtual environment.

Bibliography

[1] S. Saito, T. Simon, J. Saragih, and H. Joo, "Pifuhd: Multi-level pixel-aligned implicit function for high-resolution 3d human digitization," in *Proceedings of the IEEE Conference on Computer Vision and Pattern Recognition*, June 2020.

[2] N. Iwamoto, H. P. H. Shum, L. Yang, and S. Morishima, "Multi-layer lattice model for real-time dynamic character deformation," *Computer Graphics Forum*, vol. 34, no. 7, pp. 99–109, 2015. [Online]. Available: https://onlinelibrary.wiley.com/doi/abs/10.1111/cgf.12749

[3] H. Zhu, X. Zuo, S. Wang, X. Cao, and R. Yang, "Detailed human shape estimation from a single image by hierarchical mesh deformation," in *Proceedings of the IEEE/CVF Conference on Computer Vision and Pattern Recognition (CVPR)*, June 2019.

[4] Y. Yang, Y. Yu, Y. Zhou, S. Du, J. Davis, and R. Yang, "Semantic parametric reshaping of human body models," in *2014 2nd International Conference on 3D Vision*, vol. 2, 2014, pp. 41–48.

[5] UNCTAD, "How covid-19 triggered the digital and e-commerce turning point." https://unctad.org/news/how-covid-19-triggered-digital-and-e-commerce-turning-point, 03 2021.

[6] "Emarketer." https://www.emarketer.com/.

[7] S. Goldman, "Post-pandemic e-commerce: The unstoppable growth of online shopping," 08 2021. [Online]. Available: https://www.the-future-of-commerce.com/2021/08/03/post-pandemic-e-commerce/

[8] G. N. e. a. Tony Qui, Holger Fehlbier, "Connected capital technologies: Mergers and acquisitions tools." [Online]. Available: https://www.ey.com/en_us/strategy-transactions/connected-capital-technologies

[9] J. O. Kathy Gramling and J. Chernoff, "How e-commerce fits into retail's post-pandemic future," 05 2021. [Online]. Available: https://hbr.org/2021/05/how-e-commerce-fits-into-retails-post-pandemic-future

[10] "Engine surveyor." http://www.enginesurveyor.com/.

[11] S. Meyer, "Understanding the covid-19 effect on online shopping behavior." [Online]. Available: https://www.bigcommerce.com/blog/covid-19-ecommerce/

[12] “Digital commerce 360.” https://www.digitalcommerce360.com/.

[13] M. Stern, “Pandemic e-commerce boom a boon for retail’s biggest,” 06 2021. [Online]. Available: https://www.forbes.com/sites/retailwire/2021/06/15/pandemic-e-commerce-boom-a-boon-for-retails-biggest/

[14] “Coronavirus disease 2019 (covid-19).” [Online]. Available: https://bestpractice.bmj.com/topics/en-gb/3000201/references

[15] S. Skrovan, “Why most shoppers still choose brick-and-mortar stores over e-commerce,” 02 2017. [Online]. Available: https://www.retaildive.com/news/why-most-shoppers-still-choose-brick-and-mortar-stores-over-e-commerce/436068/

[16] G. Acosta, “Consumers still prefer physical stores,” 10 2019. [Online]. Available: https://progressivegrocer.com/consumers-still-prefer-physical-stores

[17] M. Zboraj, “Consumers still prefer in-store shopping,” 05 2021. [Online]. Available: https://progressivegrocer.com/consumers-still-prefer-store-shopping

[18] “5 reasons why customers prefer to shop in-store instead of online.” [Online]. Available: https://www.collectique.eu/en/5-reasons-why-customers-prefer-to-shop-in-store-instead-of-online/

[19] G. Pezzini, “Why physical stores are still vital for retail,” 02 2021. [Online]. Available: https://www.lsretail.com/resources/why-physical-stores-are-still-vital-for-retail

[20] T. Clark, “Benefits of physical store vs online shop,” 03 2020. [Online]. Available: https://retail-focus.co.uk/benefits-of-physical-store-vs-online-shop/

[21] S. Ward, “Brick and mortar stores vs online retail sites,” 03 2021. [Online]. Available: https://www.thebalancesmb.com/compare-brick-and-mortar-stores-vs-online-retail-sites-4571050

[22] G. Pezzini, “Why physical stores are still vital for retail,” 02 2021. [Online]. Available: https://www.aptos.com/blog/why-physical-stores-are-still-vital-for-retail

[23] B. H. H. J. e. a. Devakumar, D., “Taking ethical photos of children for medical and research purposes in low-resource settings: an exploratory qualitative study,” 2013.

[24] K. Grünberg, A. Jakab, G. Langs, T. Salas, M. Winterstein, A. Weber, M. Krenn, and O. Jimenez-del Toro, *Ethical and Privacy Aspects of Using Medical Image Data*, 05 2017, pp. 33–43.

[25] A. BANKS, “Op-ed | deepfakes and why the future of porn is terrifying,” 2018. [Online]. Available: https://www.highsnobiety.com/p/what-are-deepfakes-ai-porn/

[26] J. Christian, “Experts fear face swapping tech could start an international showdown,” 02 2018. [Online]. Available: https://theoutline.com/post/3179/deepfake-videos-are-freaking-experts-out

[27] K. Roose, “Here come the fake videos, too,” 03 2018. [Online]. Available: https://www.nytimes.com/2018/03/04/technology/fake-videos-deepfakes.html

[28] M. Schreyer, T. Sattarov, B. Reimer, and D. Borth, “Adversarial learning of deepfakes in accounting,” *ArXiv*, vol. abs/1910.03810, 2019.

[29] “International organization for standardization.” https://www.iso.org/home.html.

[30] “Iso 5971:2017.” https://www.iso.org/standard/67038.html.

[31] “Iso 8559-1:2017.” https://www.iso.org/standard/61686.html.

[32] “Iso 8559-2:2017.” https://www.iso.org/standard/64075.html.

[33] “Iso 8559-3:2018.” https://www.iso.org/standard/67334.html.

[34] T. Padmanabhan, “Geodesic distance: A descriptor of geometry and correlator of pregeometric density of spacetime events,” *Modern Physics Letters A*, vol. 35, no. 12, p. 2030008, Apr 2020. [Online]. Available: http://dx.doi.org/10.1142/S0217732320300086

[35] J. Tabak, *Geometry: The Language of Space and Form*, 2014, p. 150.

[36] L. G. Shapiro and G. C. Stockman, *Computer Vision*. New Jersey, Prentice-Hall, 2001.

[37] T. Yiu, “The curse of dimensionality,” 07 2019. [Online]. Available: https://towardsdatascience.com/the-curse-of-dimensionality-50dc6e49aa1e

[38] A. Aubel and D. Thalmann, “Realistic deformation of human body shapes,” in *Computer Animation and Simulation 2000*, N. Magnenat-Thalmann, D. Thalmann, and B. Arnaldi, Eds. Vienna: Springer Vienna, 2000, pp. 125–135.

[39] S.-Y. Baek and K. Lee, “Parametric human body shape modeling framework for human-centered product design,” *Computer-Aided Design*, vol. 44, no. 1, pp. 56 – 67, 2012, digital Human Modeling in Product Design. [Online]. Available: http://www.sciencedirect.com/science/article/pii/S0010448510002289

[40] H. Seo and N. Magnenat-Thalmann, “An automatic modeling of human bodies from sizing parameters,” in *Proceedings of the 2003 Symposium on Interactive 3D Graphics*, ser. I3D ’03. New York, NY, USA: Association for Computing Machinery, 2003, p. 19–26. [Online]. Available: https://doi.org/10.1145/641480.641487

[41] A. Volz, R. Blum, S. Häberling, and K. Khakzar, “Automatic, body measurements based generation of individual avatars using highly adjustable linear transformation,” in *Digital Human Modeling*, V. G. Duffy, Ed. Berlin, Heidelberg: Springer Berlin Heidelberg, 2007, pp. 453–459.

[42] J. Won and J. Lee, "Learning body shape variation in physics-based characters," *ACM Trans. Graph.*, vol. 38, no. 6, Nov. 2019. [Online]. Available: https://doi.org/10.1145/3355089.3356499

[43] A. Kanazawa, M. J. Black, D. W. Jacobs, and J. Malik, "End-to-end recovery of human shape and pose," in *Proceedings of the IEEE Conference on Computer Vision and Pattern Recognition (CVPR)*, June 2018.

[44] D. Anguelov, P. Srinivasan, D. Koller, S. Thrun, J. Rodgers, and J. Davis, "Scape: Shape completion and animation of people," in *ACM SIGGRAPH 2005 Papers*, ser. SIGGRAPH '05. New York, NY, USA: Association for Computing Machinery, 2005, p. 408–416. [Online]. Available: https://doi.org/10.1145/1186822.1073207

[45] M. Loper, N. Mahmood, J. Romero, G. Pons-Moll, and M. J. Black, "Smpl: A skinned multi-person linear model," *ACM Trans. Graph.*, vol. 34, no. 6, Oct. 2015. [Online]. Available: https://doi.org/10.1145/2816795.2818013

[46] A. A. A. Osman, T. Bolkart, and M. J. Black, "STAR: A spare trained articulated human body regressor," in *European Conference on Computer Vision (ECCV)*, 2020. [Online]. Available: https://star.is.tue.mpg.de

[47] E. Dibra, H. Jain, C. Öztireli, R. Ziegler, and M. Gross, "Hs-nets: Estimating human body shape from silhouettes with convolutional neural networks," in *2016 Fourth International Conference on 3D Vision (3DV)*, 2016, pp. 108–117.

[48] Y. Chen, Z. Song, W. Xu, R. R. Martin, and Z.-Q. Cheng, "Parametric 3d modeling of a symmetric human body," *Computers AND Graphics*, vol. 81, pp. 52 – 60, 2019. [Online]. Available: http://www.sciencedirect.com/science/article/pii/S0097849319300366

[49] T. Zhang, J. Wang, Q. Zhu, and B. Yin, "See through occlusions: Detailed human shape estimation from a single image with occlusions," in *2020 IEEE International Conference on Image Processing (ICIP)*, 2020, pp. 2646–2650.

[50] D. A. Hirshberg, M. Loper, E. Rachlin, and M. J. Black, "Coregistration: Simultaneous alignment and modeling of articulated 3d shape," in *Computer Vision – ECCV 2012*, A. Fitzgibbon, S. Lazebnik, P. Perona, Y. Sato, and C. Schmid, Eds. Berlin, Heidelberg: Springer Berlin Heidelberg, 2012, pp. 242–255.

[51] M. Pratscher, P. Coleman, J. Laszlo, and K. Singh, "outside-in anatomy based character rigging," in *Proceedings of the 2005 ACM SIGGRAPH/Eurographics Symposium on Computer Animation*, ser. SCA '05. New York, NY, USA: Association for Computing Machinery, 2005, p. 329–338. [Online]. Available: https://doi.org/10.1145/1073368.1073415

[52] E. W. Dijkstra, "A note on two problems in connexion with graphs," *Numerische mathematik*, vol. 1, no. 1, pp. 269–271, 1959.

[53] J. Daintith and E. Wright, “Dijkstra’s algorithm,” 2008. [Online]. Available: https://www.oxfordreference.com/view/10.1093/acref/9780199234004.001.0001/acref-9780199234004-e-1426

[54] D. Martinez, L. Velho, and P. C. Carvalho, “Geodesic paths on triangular meshes,” in *Proceedings. 17th Brazilian Symposium on Computer Graphics and Image Processing*, 2004, pp. 210–217.

[55] M. Hogg, “Pygeodesic.” https://pypi.org/project/pygeodesic/.

[56] J. S. B. Mitchell, D. Mount, and C. Papadimitriou, “The discrete geodesic problem,” *SIAM J. Comput.*, vol. 16, pp. 647–668, 1987.

[57] S. Wuhrer and C. Shu, “Estimating 3d human shapes from measurements,” *Machine Vision and Applications*, vol. 24, no. 6, p. 1133–1147, Dec 2012. [Online]. Available: http://dx.doi.org/10.1007/s00138-012-0472-y

A

Dataset Analysis Appendix

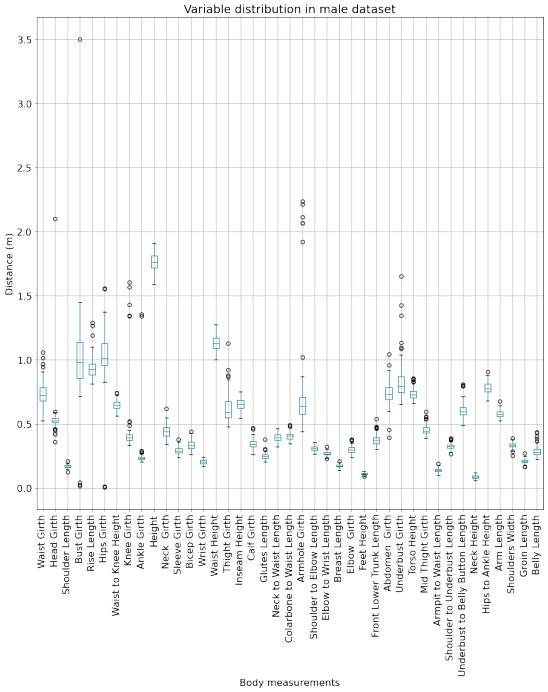

(a) Distribution of the body measurements in the male dataset.

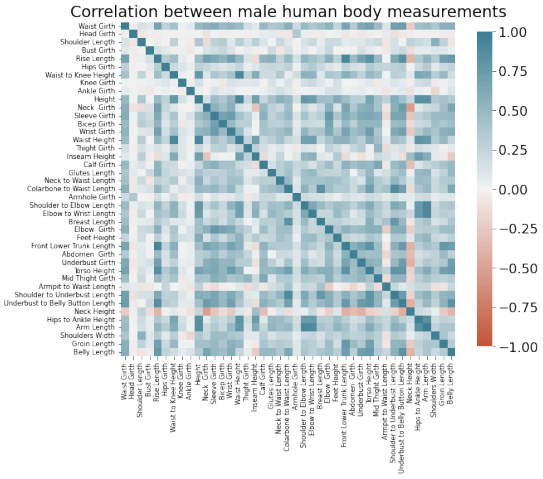

(b) Correlation of the body measurements in the male dataset.

Figure A.1: Male body measurements dataset analysis.

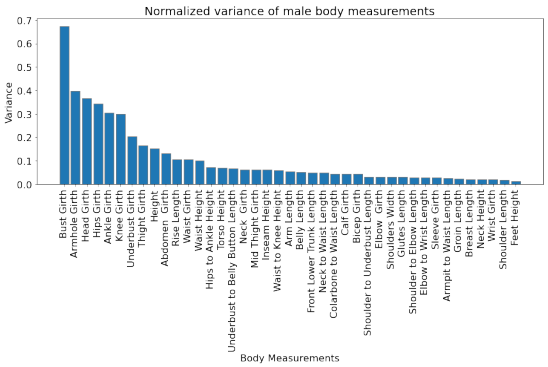

(a) Normalized values.

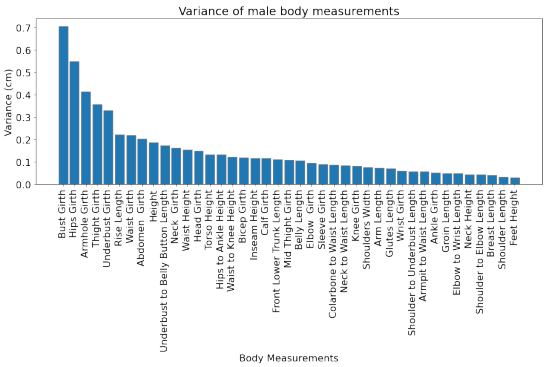

(b) Raw values.

Figure A.2: Body Measurements variance regarding the male dataset.

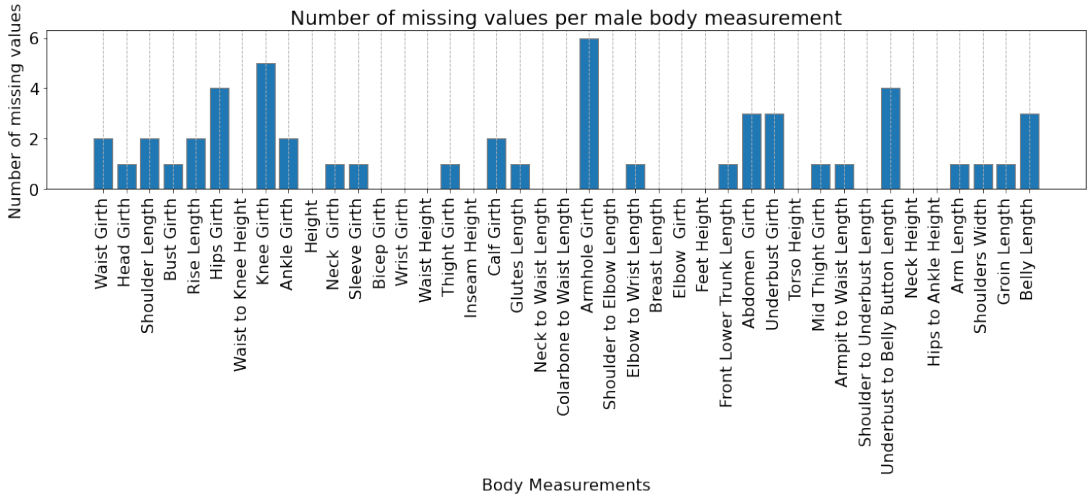

Figure A.3: Amount of missing values after replacing the outliers with missing values.

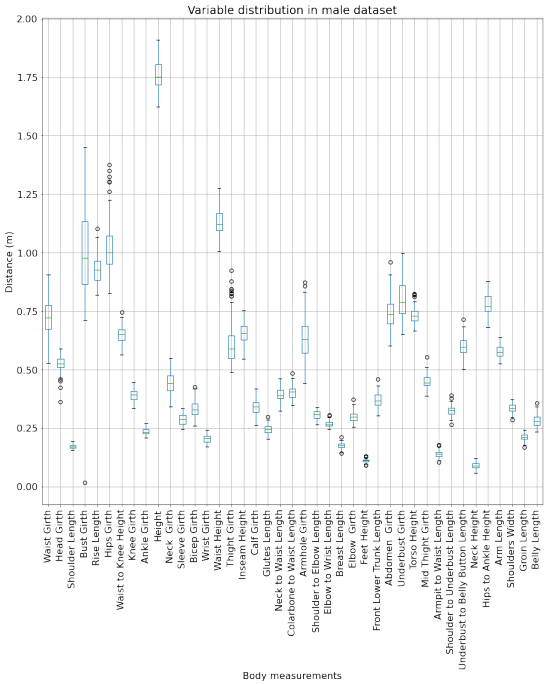

(a) Distribution of the body measurements in the male dataset after removing the outliers. Comparing with Figure A.1(a) this figure has much less outliers.

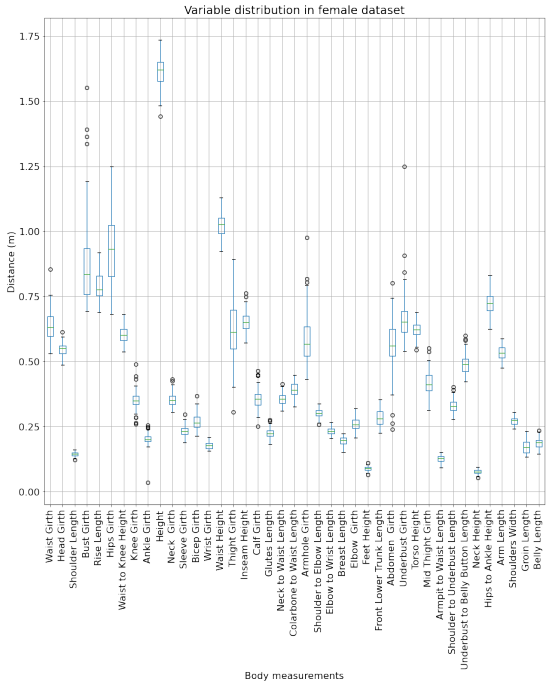

(b) Distribution of the female body measurements after removing the outliers. Comparing with Figure 4.15 this figure has much less outliers, specially in underbust girth.

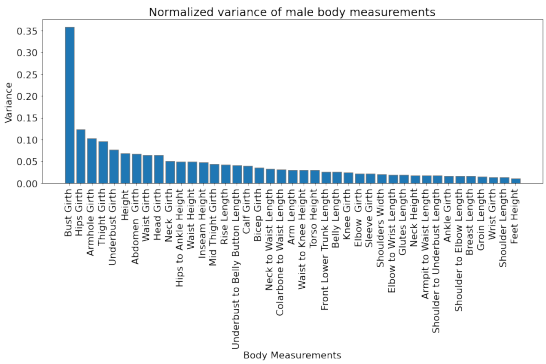

(c) Normalized values.

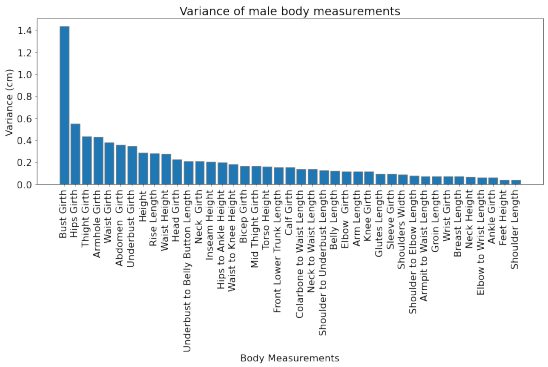

(d) Raw values.

Figure A.4: Body Measurements variance regarding the male dataset after removing the outliers.

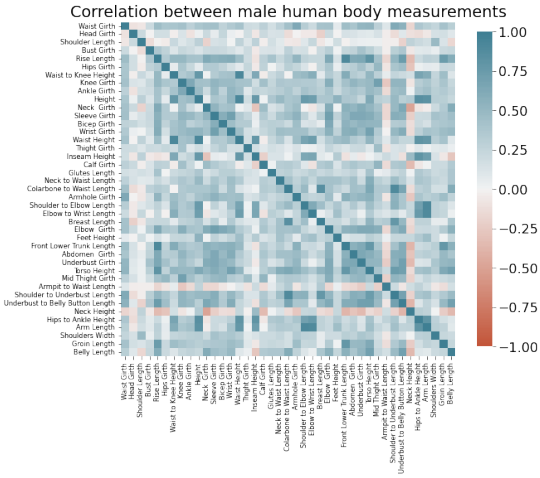

(a) Correlation of the body measurements in the male dataset after removing the outliers.

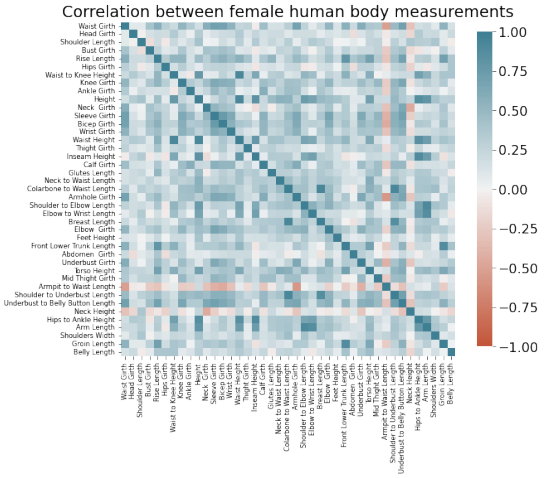

(b) Correlation of the body measurements in the female dataset after removing the outliers.

Figure A.5: Body Measurements variance regarding the male dataset after removing the outliers.

B

Body Measurements Estimations Validation

	SPRING0306 Body Measurements													
	True Value	***Estimated Value***												
		Top 10		***Top 8***		***Top 6***		***Top 4***		***Top 2***		***Selected 6***		***Selected 7***	
		LIN	*PCA*	*LIN*	*PCA*	*LIN*	*PCA*	*LIN*	*PCA*	*LIN*	*PCA*	*LIN*	*PCA*	*LIN*	*PCA*
Bust Girth	1.41	0.98	1.08	0.99	1.38	0.95	2.12	1.00	2.37	0.83	1.98	1.03	1.05	0.90	1.79
Hips Girth	1.07	1.15	1.05	1.16	1.28	1.23	1.43	1.20	1.61	1.06	1.84	0.91	1.29	1.00	1.28
Tigh Girth	0.61	0.63	0.58	0.58	0.69	0.72	0.81	0.87	0.89	0.59	1.03	0.57	0.70	0.57	0.70
Rise Length	1.19	0.95	0.84	0.92	1.02	0.93	1.15	1.02	1.23	0.89	1.31	0.78	1.15	0.80	1.04
Waist Girth	0.87	1.08	0.93	1.08	1.21	0.99	1.25	0.92	1.43	0.95	1.65	0.87	1.21	0.72	0.94
Abdomen Girth	0.93	1.08	0.96	1.08	1.26	0.94	1.28	1.16	1.47	0.97	1.70	0.88	1.26	0.89	1.26
Height	1.74	1.74	1.77	1.74	1.98	2.34	2.45	2.24	2.74	1.78	3.12	1.74	2.03	1.74	2.02
Underbust to Belly Button Length	0.76	0.63	0.65	0.64	0.72	0.54	0.70	0.58	0.77	0.57	0.85	0.48	0.69	0.54	0.69
Neck Girth	0.50	0.48	0.42	0.47	0.56	0.50	0.59	0.52	0.64	0.44	0.75	0.41	0.54	0.43	0.56
Waist Height	1.11	1.11	1.14	1.10	1.27	1.51	1.58	1.44	1.76	1.14	2.00	1.12	1.31	1.11	1.30

Table B.1: Body measurements values regarding the sample SPRING0306 estimations with 7 different subsets using the linear (*LIN*) and PCA (*PCA*) models.

	SPRING0318 Body Measurements													
	True Value	***Estimated Value***												
		Top 10		***Top 8***		***Top 6***		***Top 4***		***Top 2***		***Selected 6***		***Selected 7***	
		LIN	*PCA*	*LIN*	*PCA*	*LIN*	*PCA*	*LIN*	*PCA*	*LIN*	*PCA*	*LIN*	*PCA*	*LIN*	*PCA*
Bust Girth	1.12	0.98	1.53	1.26	1.39	0.95	2.14	1.01	1.73	0.99	2.79	0.94	1.83	0.90	1.82
Hips Girth	0.91	0.92	1.00	0.92	1.29	0.90	1.44	0.84	1.63	0.92	1.90	0.86	1.30	0.86	1.13
Tigh Girth	0.58	0.53	0.58	0.53	0.70	0.53	0.81	0.54	0.90	0.51	1.06	0.51	0.71	0.51	0.71
Rise Length	0.88	0.83	0.89	0.83	0.99	0.81	1.14	0.85	1.29	0.81	1.36	0.76	1.02	0.70	0.93
Waist Girth	0.72	0.77	0.94	0.78	1.21	0.74	1.27	0.87	1.45	0.83	1.70	0.69	1.21	0.69	1.02
Abdomen Girth	0.67	0.75	0.96	0.74	1.25	0.70	1.29	0.90	1.52	0.86	1.75	0.67	1.26	0.67	1.25
Height	1.66	1.66	1.77	1.66	2.03	1.72	2.48	1.64	2.75	1.54	3.20	1.66	2.07	1.66	2.07
Underbust to Belly Button Length	0.55	0.54	0.56	0.52	0.66	0.51	0.69	0.53	0.74	0.52	0.91	0.49	0.63	0.48	0.58
Neck Girth	0.41	0.39	0.42	0.38	0.54	0.37	0.59	0.39	0.64	0.37	0.76	0.36	0.56	0.37	0.58
Waist Height	1.05	1.05	1.14	1.06	1.30	1.11	1.60	1.06	1.77	0.99	2.06	1.07	1.34	1.07	1.33

Table B.2: Body measurements values regarding the sample SPRING0318 estimations using 7 different subsets.

	SPRING0530 Body Measurements													
	True Value	***Estimated Value***												
		Top 10		***Top 8***		***Top 6***		***Top 4***		***Top 2***		***Selected 6***		***Selected 7***	
		LIN	*PCA*	*LIN*	*PCA*	*LIN*	*PCA*	*LIN*	*PCA*	*LIN*	*PCA*	*LIN*	*PCA*	*LIN*	*PCA*
Bust Girth	0.82	0.77	1.19	0.81	1.51	0.79	1.55	0.67	1.96	0.66	2.40	1.05	1.55	1.05	1.55
Hips Girth	0.86	0.95	1.05	0.96	1.32	0.96	1.34	0.76	1.72	0.66	2.09	0.96	1.34	0.82	1.35
Abdomen Girth	0.60	0.72	0.89	0.73	1.14	0.73	1.15	0.62	1.43	0.64	1.74	0.73	1.15	0.58	1.16
Thight Girth	0.53	0.58	0.60	0.56	0.77	0.54	0.77	0.44	0.98	0.45	1.20	0.54	0.77	0.56	0.78
Height	1.63	1.63	1.62	1.63	1.92	1.63	1.99	1.19	2.66	1.21	3.24	1.63	1.99	1.63	1.98
Waist Girth	0.61	0.65	0.80	0.65	1.03	0.66	1.05	0.57	1.30	0.58	1.58	0.66	1.05	0.66	1.05
Mid Thight Girth	0.39	0.42	0.47	0.42	0.60	0.42	0.61	0.34	0.78	0.35	0.94	0.42	0.61	0.42	0.62
Waist Height	1.03	1.03	1.03	1.03	1.22	1.04	1.26	0.76	1.69	0.77	2.06	1.04	1.26	1.04	1.26
Inseam Height	0.68	0.68	0.66	0.68	0.77	0.67	0.80	0.48	1.08	0.49	1.31	0.67	0.8	0.68	0.79
Hips to Ankle Height	0.73	0.73	0.74	0.74	0.77	0.73	0.90	0.54	1.20	0.55	1.46	0.73	0.9	0.73	0.9

Table B.3: Body measurements values regarding the sample SPRING0530 estimations using 7 different subsets.

	SPRING0569 Body Measurements													
	True Value	***Estimated Value***												
		Top 10		***Top 8***		***Top 6***		***Top 4***		***Top 2***		***Selected 6***		***Selected 7***	
		LIN	*PCA*	*LIN*	*PCA*	*LIN*	*PCA*	*LIN*	*PCA*	*LIN*	*PCA*	*LIN*	*PCA*	*LIN*	*PCA*
Bust Girth	1.30	1.14	0.99	1.13	1.50	1.02	1.51	0.98	1.85	1.00	1.87	1.02	1.51	1.50	1.51
Hips Girth	0.94	1.04	1.05	1.04	1.29	1.04	1.29	0.90	1.62	0.93	1.89	1.04	1.29	0.98	1.31
Abdomen Girth	1.06	1.04	0.73	1.07	1.21	0.96	1.14	0.77	1.48	0.81	1.63	0.96	1.14	0.85	1.15
Thight Girth	0.82	0.66	0.61	0.71	0.76	0.61	0.75	0.60	0.93	0.62	1.11	0.61	0.75	0.67	0.77
Height	1.54	1.54	1.62	1.54	1.84	1.54	1.87	1.63	2.50	1.67	3.01	1.54	1.87	1.54	1.86
Waist Girth	1.14	0.92	0.80	0.93	1.03	0.84	1.04	0.72	1.23	0.79	1.49	0.84	1.04	0.89	0.09
Mid Thight Girth	0.63	0.54	0.47	0.54	0.60	0.48	0.59	0.47	0.73	0.49	0.88	0.48	0.59	0.54	0.61
Waist Height	1.00	1.00	1.03	1.00	1.17	0.97	1.19	1.03	1.59	1.06	1.91	0.97	1.19	0.98	1.18
Inseam Height	0.59	0.59	0.66	0.61	0.73	0.61	0.75	0.66	1.02	0.67	1.22	0.61	0.75	0.60	0.74
Hips to Ankle Height	0.68	0.68	0.74	0.71	0.84	0.69	0.85	0.73	1.13	0.75	1.36	0.69	0.85	0.70	0.84

Table B.4: Body measurements values regarding the sample SPRING0569 estimations using 7 different subsets.